Analysis of Stirling engine and comparison with other technologies using low temperature heat sources

Tamrat Abishu Gelu

Thesis to obtain the Master of Science Degree in

Energy Engineering and Management

Supervisors: Prof. João Luís Toste de Azevedo

Prof. Edgar Caetano Fernandes

Examination Committee:

Chairperson: Prof. José Alberto Caiado Falcão de Campos

Supervisor: Prof. Edgar Caetano Fernandes

Member of the committee: Prof. Carlos Augusto Santos Silva

May 2014

Acknowledgement

This project work is performed for the fulfillment of the requirements for the Degree of Master of Science in Energy Engineering and Management. This master thesis was supervised by the late Professor Dr. Joao Luis Toste. I would like to express my deepest gratitude to him for giving me the opportunity to work with him on the interesting field of low grade heat recovery technologies. His guidance, support and patience were very valuable. He was very exceptional person. May his soul rest in peace.

I am very thankful to Professor Falcão de Campos for his follow up and helping me solve academic as well as administrative issues. Without his follow up and support it would not be possible for me to finish this thesis.

A special thanks to the KIC InnoEnergy – M.Sc. Renewable Energy program for providing me with a scholarship to study in prestigious universities in Europe.

Finally, I would like to thank my family and friends who are always around and supporting me during the course of this M.Sc. program.

Abstract

This master thesis report presents the work performed on recovery of low grade heat into electricity using two different technologies. The two technologies studied are the Stirling engine and the Organic Rankine Cycle (ORC).

The Stirling engine is studied for conversion of waste heat with temperature of 250^0C. An isothermal model of the engine is assumed and a first order thermodynamic cycle analysis is performed. The effect of regenerator, hot and cold space dead volumes are taken into account in the analysis. Detailed regenerator thermodynamic analysis is also carried out on different screen mesh surfaces and the best screen mesh is selected. The performance of the engine is evaluated for different values of hot temperature, regenerator effectiveness and phase angle. 2.2kW power is produced at engine efficiency of 20.2%.

The ORC system is studied for conversion of solar thermal energy into electricity. The solar thermal system is designed using Polysun software to provide hot water at 90^0C to the ORC evaporator. An ORC with a preheater is modeled in EES software. Six different organic working fluids (R123, R134a, R245fa, R600, n-Pentane and Isobutane) are selected and studied under the same input variables. The first and second laws of thermodynamics are used for performance evaluation of the ORC. The effect of the turbine inlet temperature and pressure on the performance of the ORC is evaluated using the selected fluids. The solar ORC is designed for 2kW power output. Fluids R123 and n-Pentane have showed higher thermal efficiency and lower exergy destruction rate, and fluid R134a has the least turbine exit volume flow rate.

Resumo

Este trabalho de mestrado apresenta um estudo realizado sobre a conversão de calor de "baixa qualidade" em eletricidade, com base no ciclo de Stirling e no ciclo de Rankine orgânico (ORC).

O motor Stirling foi estudado para a conversão de calor quando a temperatura da fonte quente é de 250^0C, sendo modelado como um sistema isotérmico de 1ª ordem onde o efeito do regenerador (análise da tela que controla a transferência de calor) e os volumes "mortos" dos reservatórios de energia são devidamente contabilizados. O desempenho do motor é avaliado para diferentes valores da temperatura do ar quente, a eficiência do regenerador e do ângulo de fase. Conclui-se que a maxima potência de 2.2kW é atingida com um redimento de 20.2% .

O ciclo ORC foi estudado para a conversão de energia solar térmica em energia elétrica e projectado para uma potência de 2kW. O sistema solar térmico foi projetado usando o programa computacional Polysun para fornecer água quente a 90^0C para o evaporador do ciclo ORC. O ciclo ORC com um pré-aquecedor foi modelado no software EES, para seis diferentes fluidos de trabalho orgânicos (R123, R134a, R245fa, R600, n- pentano e isobutano) e em condições de operação semelhantes. Foram avaliados o efeito da temperatura de entrada da turbina e da pressão sobre o desempenho da ORC, utilizando os fluidos seleccionados. O funcionamento do ciclo com os fluidos R123 e n- Pentano mostraram maior eficiência térmica e menor taxa de destruição de exergia e com a utilização do fluido R134a verificou-se que o caudal volumétrico à saida da turbina é o menor .

Por fim, com os resultados da análise termodinâmica entre as duas tecnologias verifica-se que o ciclo ORC tem um melhor desempenho na gama das temperaturas mais baixas e que o motor Stirling apresenta melhor desempenho na gama da temperaturas mais altas.

Table of Contents

1. Introduction

Fast development of industry has resulted in extensive use of fossil fuel for electricity and heat production. This in turn has caused serious environmental problems like global warming, ozone layer destruction, acid rain and contamination of lands and seas. These problems associated with use of fossil fuel have focused attention on new energy sources and on effective means of energy conversion and utilization. Use of renewable sources of energy such as solar energy, wind energy, biomass energy and geothermal energy as well as waste heat conversion are solutions to the problems caused by fossil fuel. The main drawbacks associated with the use of renewable sources of energy are lack of technology to efficiently convert the energies and high initial capital cost to install the conversion technologies.

In this report two different types of technologies for conversion of low grade heat (waste heat) into electricity are studied. The two conversion technologies are: the Stirling engine and the Organic Rankine Cycle (ORC). Compared to the Stirling engine, the ORC is a well developed technology for conversion of low grade heat into power. The Stirling engine is a technology that is under development, but it is simple to construct. In terms of power production capacity, ORC is used for medium power generation (~200 kWel) and Stirling is used for small scale power production (~100 kWel).

Several research works have been reported in the literature on the performance of Stirling engine [1 - 4] and ORC [5 - 11] technologies for low grade heat conversion. Energy from solar, geothermal and waste heat from industries are the main sources of heat for both technologies. One of the measures of their performance is how efficient they are in converting low temperature heat into power. Reports suggest that ORC is capable of converting low grade heat with temperature as low as 55^0C [12, 13]. The Stirling engine can run with very low temperature difference up to 10^0C, but to produce useable power it requires higher temperature more than 100^0C.

The ORC uses organic fluids with low critical temperatures (e.g. R123, R134a, Butane, CF31, etc.). Use of organic fluid with low critical temperature improves the performance of the ORC and makes it possible to convert very low temperature waste heat. The Stirling engine uses gases with low heat capacity like helium, hydrogen, air, etc so that a given amount of transferred heat leads to a large increase in pressure.

In the present study, detailed thermodynamic analysis is made for the two technologies. The Stirling engine is assumed to be driven by waste heat from industries and the ORC is driven by solar thermal energy. The waste heat from industries is assumed to provide temperature at 250^0C. The cooler side temperature is 80^0C. The solar thermal system provides hot water at 90^0C to the evaporator of the ORC and the ORC rejects heat at 35^0C. The solar ORC system is designed to be used in Ethiopia, East Africa, where there is high solar radiation almost all year round. The power output from the Stirling engine is 2.2 kW and from the ORC is 2 kW.

1.1. Objective

This master thesis has two main objectives. The first objective of the work is to adapt existing models to describe the process in the Stirling engine. Based on this model an investigation of the effect of the regenerator characteristics should be carried out. The model should allow for the calculation of the engine efficiency as a function of the operating conditions that reproduce the performance of the existing engines.

A second objective of the work is the comparison of the performance of the Stirling engine with other cycles that may operate with low temperature heat sources such as the ORC (Organic Rankine Cycle) using different fluids. For this comparison data from a literature review will be used and a model for the cycle including the heat transfer in the main heat exchangers.

The thesis should also address how solar energy can be integrated in the systems under consideration.

1.2. Structure

This thesis report is structured in to four main parts, each one addressing the following:

The first part highlights the concept of low temperature heat source and the technologies available for conversion.

The second part presents detailed thermodynamic analysis of the Stirling engine including the regenerator.

The solar ORC system is given in the third part. Solar thermal system and organic working fluid selection is discussed.

The last part presents conclusions based on the results of the analysis made and suggestions for future work.

2. Heat engines using low-grade heat sources

A low-grade heat source also called waste heat or secondary heat is a low- and mid- temperature heat that has less exergy density or higher entropy than the original energy source and cannot be converted into other source of power (e.g. electrical, mechanical) efficiently by conventional heat engines. There is no specific temperature range to specify the temperature of low-grate heat but in general heat source up to 370^0C is considered as a low-grade heat source [14]. The main sources of low-grade heat are renewable energy sources, such as solar thermal and geothermal, and vast amounts of industrial processes, such as power plants, oil refining, steel making, etc. They are potentially promising energy sources capable, in part, to meet the world electricity demand.

2.1. Low-grade temperature heat conversion technologies

The low and moderate temperature heat from low-grade heat sources cannot be converted efficiently to electrical power by conventional power generation methods. As a result, a large amount of low and moderate temperature heat is simply wasted or released to the atmosphere. This waste heat has significant potential to generate electrical power with utilization of suitable technologies. Therefore, research on how to convert these low-grade temperature heat sources into electrical power is of great significance. Several researchers have proposed and studied various thermodynamic cycles for the conversion of low-grade heat sources into electricity. The most common cycles used for this application are the organic Rankine cycle, supercritical Rankine cycle, Kalina cycle, Goswami cycle, trilateral flash cycle and Stirling engine.

2.1.1. Organic Rankine cycles

This is the derivative of the Rankine cycle which applies the principle of the steam Rankine cycle, but instead of steam it uses organic working fluids with low boiling point to recover heat from lower temperature heat source. The

organic Rankine cycle is the most diversely used cycle for low-grade heat application. The cycle consists of four basic components. These are: a pump, a boiler, an expansion turbine and a condenser.

Theoretically, ORC's provide much less power than Kalina cycle. But practically, under identical conditions of ambient temperature and cooling systems, Pippo [20] has shown that the difference in performance is only 3% in favor of Kalina cycle. However, the organic Rankine cycle is much less complex and needs less maintenance.

There are three subdivisions of ORC based on the critical working pressure of the organic fluid. These are:
Subcritical cycle: where the working pressure is below the critical pressure.
Supercritical cycle: where the pressure is always above the critical pressure.
Transcritical cycle: the low pressure is below the critical pressure and the high pressure is above the critical one.

Detailed study on the thermodynamic cycle analysis and working fluid selection for ORC is given in the following sections.

2.1.2. Kalina Cycle

The Kalina cycle is a type of Rankine cycle with some modification. The technology was first developed in late 1970's and early 1980's by Dr. Alexander Kalina. It uses a working fluid comprised of at least two different components, typically water and ammonia.

The ratio between those fluids varies in different parts of the system to decrease thermodynamic irreversibility and therefore increase the overall thermodynamic efficiency. The Kalina cycle is claimed to provide 15 – 50% more power output relative to organic Rankine cycles for the same heat input [15 - 18]. Some of the main drawbacks of this technology are the need of high vapor fraction in the

boiler and the corrosive behaviour of ammonia which can damage copper, zinc and mild steel.

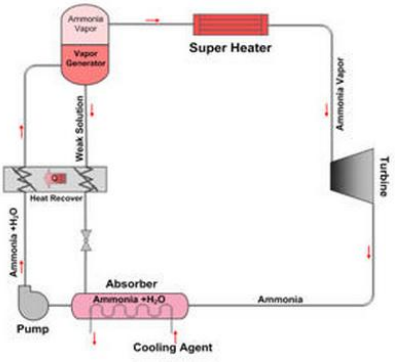

Fig. 1. Basic configuration of Kalina cycle [19].

2.1.3. Goswami cycle

This cycle was developed by Dr. Yogi Goswami in 1998. Like the Kalina cycle it uses binary working fluids, such as ammonia-water, but produces power and refrigeration simultaneously in one loop. The Goswami cycle is a combination of Rankine power cycle and an absorption cooling cycle. The main advantages of this cycle are [19]: (a) the production of power and cooling in the same loop, (b) it has design flexibility to produce any combination of power and refrigeration, (c) the efficient conversion of moderate temperature heat sources, and (d) the possibility of improved resource utilization compared to separate power and cooling systems.

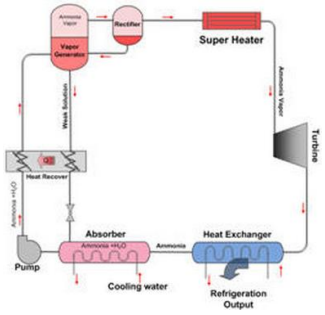

Fig.1. Basic configuration of combined power and cooling cycle [ref 19].

2.1.4. Trilateral Flash cycle

Among the thermodynamic cycles used for low-grade heat conversion, the Trilateral Flash cycle (TFC) has a unique feature in which expansion starts from the saturated liquid rather than the saturated, superheated or supercritical vapor phase. The main advantage of this cycle is that the boiling part is avoided and as a result the heat transfer from a heat source to a liquid working fluid is achieved with almost perfect temperature matching, which in turn results in minimization of irreversibilities. Some studies has shown that up to 85% more power could be recovered than using ORC or flash steam system [19]. The main challenge associated to this technology is the lack of suitable expander which can handle a two phase flow and high adiabatic efficiency.

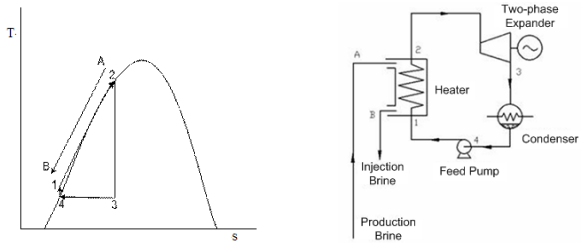

(a) (b)

Fig. 2. Trilateral flash cycle, (a) the process in T-s diagram, (b) the basic configuration [19].

2.2. Solar-thermal system

The solar energy is harnessed to provide DHW for a residential building. The DHW in turn is used to heat the working organic fluid in the evaporator. Flat plate collector, evacuated tube collector, parabolic dish, parabolic trough and solar tower are some of the well-proven technologies for harnessing solar energy for thermal energy (heat) requirement in residential buildings, industries and commercial sectors. The capacity (efficiency) of a solar-thermal system is affected by several factors which include: atmosphere, geographical location, number of solar hours, season and latitude, angle of incidence, pollution, etc.

3. The Stirling Engine

3.1. Introduction

Robert Stirling invented the Stirling engine in 1816 in Scotland. Until the early 1900s the Stirling engine has sought substantial commercial success [21]. But rapid development of internal-combustion engine and the electric motor in the beginning of the 19th century had severely hampered further development of the Stirling engine. In late 1900s, due to fuel crisis and the growing demand for energy and increasing environmental concern a wide range of investigations in material technology have been made on the development of the Stirling engine. In recent years researchers and commercial companies have been showing interest in developing the Stirling engine due to several reasons. Some of the reasons include: its simplicity in construction, multi-fuel capability, compactness, low noise, high heat efficiency and reliability. In addition, it can be used for applications in heating and cooling, combined heat and power, nuclear and solar power generation, heat pump, low temperature difference engine and automotive, marine and aircraft engines.

3.2. Stirling cycle description

The Stirling engine works on a closed regenerative thermodynamic cycle with external heat input between minimum and maximum temperatures, T_C (T_{min}) and T_E (T_{max}). It has three different configurations: alpha, beta and gamma. Each of these configurations is explained later in this report. The three configurations are different in their mechanical design but their thermodynamic cycles are the same. The thermodynamic cycle in P-V and T-S diagram is shown in Fig.3. To explain the working process of a Stirling engine, a representative diagram is shown in Fig 4. It has four processes namely isothermal compression and expansion and isochoric heat addition and rejection processes [21]. The working fluid undergoes a cyclic compression and expansion process between the

temperature limits so that there is a net conversion of heat to work or vice versa. The working process of a Stirling engine is explained below as given in [21].

Consider a cylinder containing two opposed pistons with a regenerator between the pistons as shown in Fig. 4. The regenerator is like a thermal

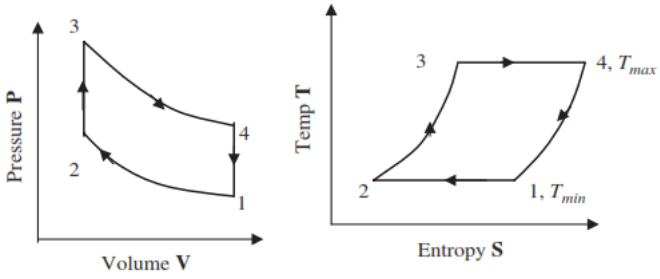

Fig. 3. P-V and T-S diagram for Stirling cycle engine [21].

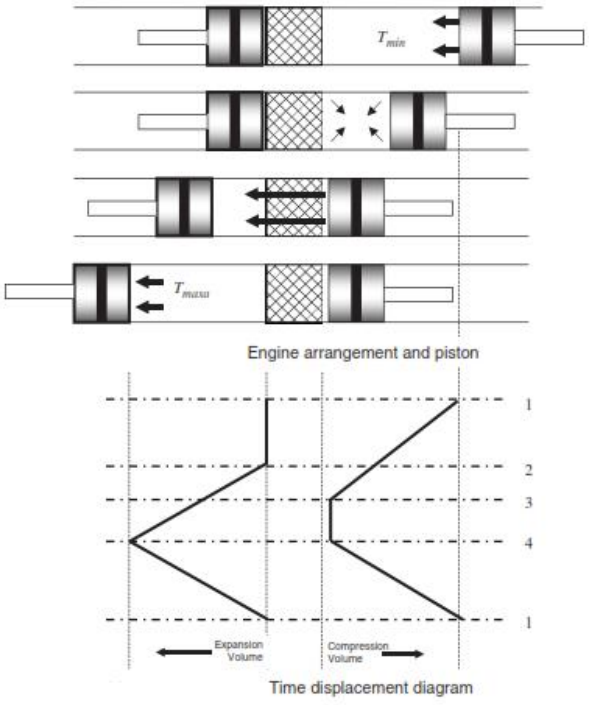

Fig. 4. Stirling cycle engine [21].

sponge alternatively absorbing and releasing heat, it is a matrix of finely divided metal in the form of wires or strips. The volume between regenerator and the right side piston is expansion volume and between regenerator and left side piston is compression volume. Expansion volume is maintained at high temperature and compression volume is maintained at low temperature. The temperature gradient of (T_{max}-T_{min}) between the ends of regenerator is maintained.

3.3. Engine thermodynamic cycle

To start with a cycle we assume that the compression space piston, in Fig. 4, is at outer dead point (at extreme right side) and the expansion space piston is at inner dead point close to regenerator. All working fluid is in the cold compression space. The compression volume is at maximum and the pressure and temperature are at their minimum values represented by point 1 on PV and TS diagram (Fig.3). The four processes of the thermodynamic cycle are:

Process 1–2, isothermal compression process: During compression process from 1 to 2, compression piston moves towards regenerator while the expansion piston remains stationary. The working fluid is compressed in the compression space and the pressure increases from P_1 to P_2. The temperature is maintained constant due to heat flow from cold space to surrounding. Work is done on the working fluid equal in magnitude to the heat rejected from the cycle. There is no change in internal energy and there is a decrease in entropy.

Process 2–3, constant volume regenerative transfer process: In this process, both pistons move simultaneously, i.e. compression piston towards regenerator and expansion piston away from regenerator, so that the volume between pistons remains constant. The working fluid is

transferred from compression volume to expansion volume through porous media regenerator. The temperature of working fluid increases from T_{min} to T_{max} by heat transfer from regenerator matrix to working fluid. The gradual increase in temperature of working fluid while passing through regenerator causes increase in pressure. No work is done and there is an increase in the entropy and internal energy of the working fluid.

Process 3– 4, isothermal expansion process: In this process, the expansion piston continues to move away from the regenerator towards outer dead piston while compression piston remains stationery at inner dead point adjacent to regenerator. As the expansion proceeds, the pressure decreases as volume increases. The temperature maintained constant by adding heat to the system from external source at T_{max}. Work is done by the working fluid on piston equal in the magnitude to the heat supplied. There is no change in the internal energy, but an increase in the entropy of the working fluid.

Process 4–1, constant volume regenerative transfer process: In this process, both pistons move simultaneously to transfer working fluid from expansion space to compression space through regenerator at constant volume. During the flow of working fluid through regenerator, the heat is transferred from the working fluid to the regenerator matrix reducing the temperature of working fluid to T_{min}. No work is done; there is a decrease in the internal energy and the entropy of the working fluid.

3.4. Engine configuration

Based on the forms of cylinder coupling Stirling engines are classified into three types of configurations [21, 22]: alpha configuration, beta configuration and

gamma configuration. Each configuration has different mechanical design characteristics but the thermodynamic cycle is the same for all.

3.4.1. Alpha configuration

The present study deals with this type of Stirling engine configuration. Alpha type engines features two pistons, called hot and cold pistons, in two separate cylinders as shown in Fig. 5. The two pistons shuttle the working fluid from one cylinder to the other. Alpha engines have the advantage of interconnecting number of cylinders in such a way that the compression space of one cylinder is connected to the expansion space of the adjacent cylinder via a series connected cooler, regenerator and heater. This compounding of cylinders is important to attain extremely high specific power output from alpha engines, and it can be used for automotive engines [21]. The pistons are typically driven by a swash plate, resulting in a pure sinusoidal reciprocating motion having a 90^0 phase difference between the adjacent pistons [21].

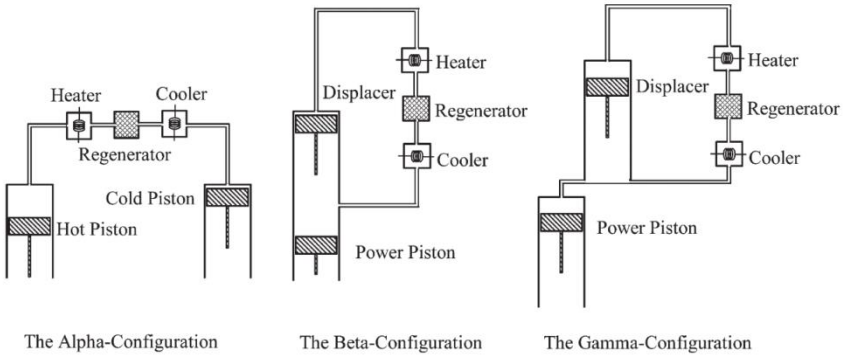

Fig. 5. Three basic mechanical configurations for Stirling engine [22].

3.4.2. Beta configuration

In this configuration the displacer and the power piston are accommodated in same cylinder as shown in Fig. 5. The space swept by the underside of the

displacer and the topside of the power piston forms the compression space. The working fluid is moved, by the displacer, between the hot space and cold space via the heater, regenerator and cooler. To maintain the required phase angle, the displacer and power piston are connected to the crankshaft by separate linkages.

3.4.3. Gamma configuration

It has similar arrangement with the Beta engine configuration but the displacer and the power piston are kept in two separate cylinders, called displacer cylinder and compression cylinder respectively, as shown in Fig. 5. The two cylinders are interconnected through cooler, regenerator and heater. This type of configuration has the advantage of good self-pressurization and with a double-acting piston arrangement it has theoretically the highest possible mechanical efficiency [22].

3.5. Working fluids and heat source

Compressible fluids such as air, helium, hydrogen, nitrogen and vapor can be used as working fluids for the Stirling engine. In general, because of their higher heat transfer capabilities than other fluids hydrogen and helium are used. Hydrogen has high thermal conductivity and low viscosity which allows the engine to run faster than with other gases but due to its flammability it is not safe to work with. Helium is an inert gas and safer to work with but relatively expensive.

The Stirling engine is an external combustion engine. The heat source for a Stirling engine can be solar radiation [23, 24, 25] combustible materials [26, 27], geothermal steam and hot water, exhaust, radioisotope energy and so on.

3.6. Modeling methods

Different assumptions are employed in the Stirling engine analysis. The degree of difficulty of the analysis depends on these assumptions. The techniques of analysis for Stirling engines can be categorized into four [28] as follows:

Zero Order Analysis: using Beale formula which gives the engine performance.

First Order Analysis: (Schmidt analysis) was done in 1871 by Gustav Schmidt in which he obtained closed-form solutions for the special case of sinusoidal volume variations and isothermal hot and cold spaces. This is a loss free analysis.

Second Order Analysis (decoupled methods): This level of analysis may be based on an adiabatic analysis that subtracts losses caused by heat transfer and flow power losses. It relies on a modified Schmidt analysis and requires nonlinear time integration of the model equations. It assumes adiabatic expansion and compression regions.

Third order analysis (coupled methods): uses control volumes or nodes to directly solve one-dimensional (2D and 3D) governing equations. This requires the use of computer codes such as GLIMPS, HFAST, CAST, FLUENT, STAR, CFX.

In the present study the first order analysis is performed for the thermodynamic modeling of an alpha type of Stirling engine, taking into account the dead volumes of the regenerator, hot space and cold space.

3.7. Regenerator

The regenerator is a cyclic heat sponge device. In the first part of the cycle the hot gas flows through the regenerator from the heater to the cooler, and in so doing transfers heat to the regenerator matrix. This is referred to as a "single blow". Subsequently during the second part of the cycle the cold gas flows in the reverse direction, absorbing the heat that was previously stored in the matrix. Thus at steady state the net heat transfer per cycle between the working gas and

the regenerator matrix is zero.

3.8. Dead volumes and regenerator ineffectiveness

It is evidenced that a real Stirling engine must have some unavoidable dead volume. Total dead volume is defined as the sum of Stirling engine void volumes. The dead volumes are considered for regenerator, cold and hot spaces. In normal Stirling engine design practice, the total dead volume is approximately 58% of the total volume [29].

In the ideal Stirling cycle, it is assumed that the total heat rejected during process 4-1 is absorbed by the regenerator and then released to the working fluid during the process 2-3. In reality, it is not possible to build the ideal regenerator, and all of the regenerators due to their structure and type of materials used have deficiency (inefficiency). So, an imperfect regenerator cannot absorb the total heat released during process 4-1, and consequently cannot provide the total required heat of process 2-3. In the present study, the imperfection of the regenerator is taken into account and the temperatures of working fluid at exit of the imperfect regenerator are noted as T_3' and T_1' as shown in Fig. 4.

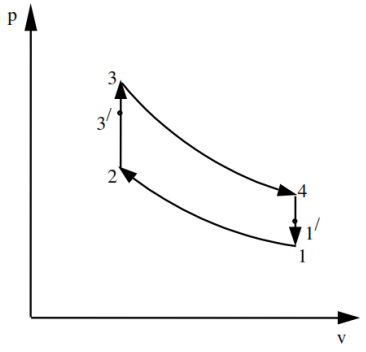

Fig. 4. P-V diagram showing regenerator exit points.

The theoretical thermal efficiency of Stirling cycle equals that of the hypothetical Carnot cycle thermal efficiency. However, in practice due to irreversibilities caused by flow losses, gas leakage, heat losses, discontinuous

piston motion or/and dead volume effects reduce the actual thermal efficiency of a Stirling engine.

3.9. Regenerator packing geometries

In cryogenic applications there are four commonly used regenerator packing geometries. Each of these geometries are illustrated in Fig. 7.

Annular gap: It has simple geometry (cylindrical), and introduces a low pressure drop and minimum dead volume, Fig. 7 (a). It has limited amount of heat transfer area and minimum surface capacity (thermal penetration depth) of the walls to store heat.

Wire mesh screen: Woven wire mesh screen is the most commonly used regenerator material [30], Fig. 7 (b). It is selected for regenerator application because of its high heat transfer area with minimum pressure drop, it is readily available in useful mesh sizes from 50 mesh (50 x 50 openings per inch) to over 250 mesh. It is available in many different materials, it is relatively inexpensive to use, and the smaller diameter and high thermal conductivity of the wire used to weave the screens provides full utilization of the thermal capacity of the material. Detail analysis of wire mesh screen is given later in this report.

Spherical particle bed: Fig. 7 (c), these are generally used for low temperature applications where specific heats of commercially available materials drop to values that are close to the working fluid specific heat [30]. Some special materials compounds, mostly available in spherical form, which have higher capacity at low temperatures, are used to improve its effectiveness. They are mostly used for applications involving temperature below 25K where viscosity of the fluid is low, which otherwise increase the pressure drop.

The ribbon: Shown in Fig. 7 (d) is the dimpled ribbon regenerator. This regenerator is produced by introducing dimples or etching on the surface of the material and then rolled to obtain a cylindrical shape which can fit into the cylinder. The working fluid flows in axial direction between the concentric annular channels formed by the standoffs. They introduce low pressure drop compared to wire mesh screen regenerators. However, it has low porosity and uneven flow distribution [30].

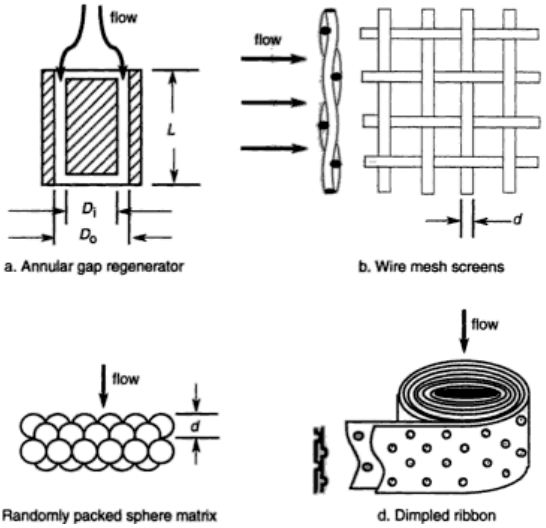

Fig. 7. Common regenerator matrix geometries [30].

The type of matrix geometry used for a regenerator has a significant effect on its effectiveness. In general, regenerator matrix geometry should have the following characteristics for a better efficiency [31]:

- Maximum heat transfer area
- Minimum axial conduction
- Minimum pressure drop loss
- High heat capacity
- Minimum void (dead) volume

Among these, heat transfer area to fluid pressure drop ratio is the critical

parameter in the definition of the effectiveness of a regenerator pack. Maximizing this ratio with minimum cost is a major design consideration [31].

3.10. Regenerator material

Several materials can be used for the regenerator matrix, such as stacked screen, packed balls, steel wool, metal foils, steel felt, fine pipes, spring mesh, wire mesh and parallel plates etc. The performance of the engine depends on the performance of the matrix material. The best candidate material must have high heat storage capacity, improved heat transfer coefficient, low conductivity and small diameter. For this reason stainless steel and ordinary steel are the most suitable materials to make the regenerator matrix [21, 30]. In the present study Stainless steel Grade-316 is used for the screen materials. The matrix must have large heat transfer area to establish the minimum temperature deference between matrix and working gas. The following are the desirable characteristics of regenerator matrix [21].

1. For maximum heat capacity - a large, solid matrix is required.
2. For minimum flow losses - a small, highly porous matrix is required.
3. For minimum dead space - a small, dense matrix is required.
4. For maximum heat transfer - a large, finely divided matrix is required.
5. For minimum contamination - a matrix with no obstruction is required.

Hence the design of regenerator is a matter of optimization of regenerator volume for best values of above parameters.

3.11. Regenerator effectiveness and thermodynamic analysis

The two main geometrical parameters used in the description of screen regenerators are the porosity and area density. They are defined as [30]:

$$\alpha = \frac{total\ volume\ of\ connected\ void\ spaces}{total\ volume\ of\ the\ matrix} = porosity \qquad (1)$$

$$\beta = \frac{total\ surface\ area\ of\ connected\ voids}{total\ volume\ of\ the\ matrix} = area\ density \quad (2)$$

From the above two parameters, an important relationship for the hydraulic radius, which is one fourth of the hydraulic diameter, d_h, for a screen packing is obtained as:

$$r_h = \frac{\alpha}{\beta} \quad (3)$$

Alternatively, the hydraulic radius can be expressed in terms of an average free flow cross-sectional area, A_{ff}, the total heat transfer area, A_{wg}, and regenerator length, L. This is obtained by setting the volume of the matrix flow passage equal to the porosity times the volume of the regenerator as:

$$A_{ff}L = \alpha A_r L \quad (4)$$

$$\beta = \frac{A_{wg}}{A_r L} \quad (5)$$

From the above two equations:

$$r_h = L\left(\frac{A_{ff}}{A_{wg}}\right) \quad (6)$$

The porosity of the screen regenerator is found by weighing the packed regenerator and subtracting the tare weight of the regenerator canister:

$$\alpha = 1 - \frac{m_m}{\rho_m V_r} \quad (7)$$

where m_m is the mass of the packed matrix material, ρ_m is the density of the packing (matrix), and V_r is the regenerator volume.

The area density is computed from the screen dimensions shown in Fig. 8 by calculating the circumferential heat transfer area of the wires and the total volume encompassed in one segment of screen mesh:

$$\beta = \frac{A_{wg}}{V_r} = \frac{1/2(wire\ wetted\ perimeter)(length\ of\ the\ opening)(4\ sides)}{(volume\ encompassing\ the\ wires)} \quad (8)$$

$$\beta = \frac{1/2(\pi d)(1/n)(4)}{(1/n)^2 t_s} = \frac{2\pi dn}{t_s} \quad (9)$$

where d is the wire diameter, t_s is the screen thickness, and n is the mesh size.

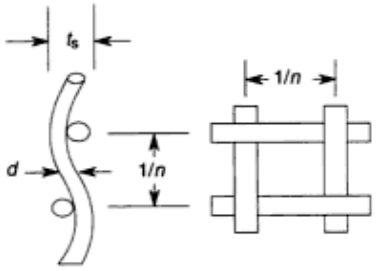

Fig. 8. Geometry of woven screen [30].

The regenerator effectiveness is usually defined on an enthalpy basis in terms of a regenerator effectiveness ε as follows:

$$\varepsilon = \frac{actual\ enthalphy\ change\ of\ gas\ during\ a\ single\ blow\ through\ the\ regenerator}{equivalent\ maximum\ theoretical\ enthalphy\ change\ in\ an\ ideal\ regenerator}$$

An equivalent definition in the context of the ideal adiabatic model is proposed, which represents the limiting maximum performance measure, as follows:

$$\varepsilon = \frac{amount\ of\ heat\ transfered\ from\ matrix\ to\ gas\ during\ a\ single\ blow\ through\ the\ regenerator}{equivalent\ amount\ of\ heat\ transfered\ in\ the\ regenerator\ of\ the\ ideal\ adiabatic\ model} \qquad (10)$$

The regenerator effectiveness ε thus varies from 1 for an ideal regenerator (as defined in the ideal adiabatic model) to 0 for no regenerative action.

The regenerator effectiveness can also be expressed in terms of the temperature profile of the 'hot' and 'cold' gas streams with respect to the regenerator matrix, Fig. 9. Assuming an equal difference in temperature ΔT on the hot and the cold sides, and linear temperature profiles, leading to the definition of regenerator effectiveness ε in terms of temperatures.

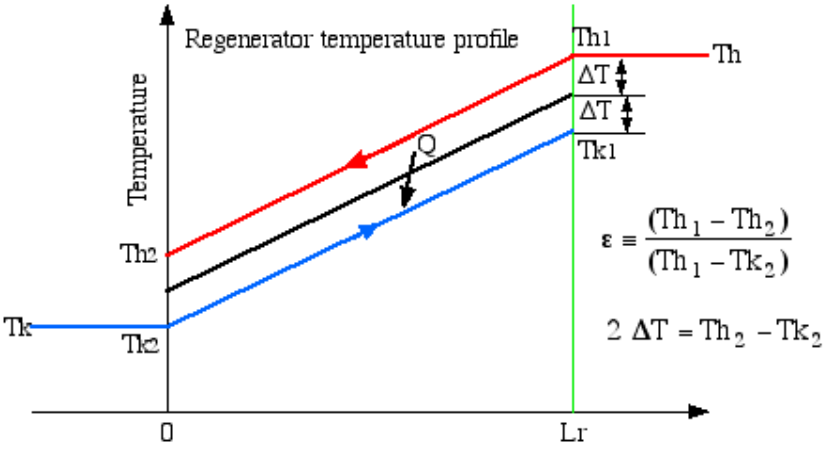

Fig. 9. Regenerator temperature profile

Combining the two equations in Fig. 9, we obtain:

$$\varepsilon = \frac{1}{1+\frac{2\Delta T}{(T_{h1}-T_{h2})}} \tag{11}$$

Now, from energy balance considerations of the hot stream, the change in enthalpy of the hot stream is equal to the heat transfer from the hot stream to the matrix, and subsequently from the matrix to the cold stream, thus:

$$\dot{Q} = c_p \dot{m}(T_{h1} - T_{h2}) = 2hA_{wg}\Delta T \tag{12}$$

Where $\dot{Q}$ (Watts) is the heat transfer power, h is the overall heat transfer coefficient (hot stream / matrix / cold stream), A_{wg} refers to the wall/gas, or "wetted" area of the heat exchanger surface, c_p the specific heat capacity at constant pressure, and $\dot{m}$ (kg/s) the mass flow rate through the regenerator. Substituting in the effectiveness equation we obtain:

$$\varepsilon = \frac{1}{1+\frac{c_p \dot{m}}{h\, A_{wg}}} \tag{13}$$

Hence, the regenerator heat transfer coefficient, h, and the mass flow rate through the generator must be known to determine the effectiveness of the regenerator.

The mass flow rate through the regenerator is calculated from engine speed, swept volume and density of working gas, as follows:

Mass of gas that flows per half cycle:

$$m_f = \rho_g V_{swept} \tag{14}$$

The mass flow rate per second, $\dot{m}$, becomes:

$$\dot{m} = 2 * \acute{n}_s * m_f \tag{15}$$

Where $\acute{n}_s$ is the engine speed in cycle per second.

The heat transfer coefficient is determined using the well-known Reynolds analogy. This analogy relates the heat transfer to fluid friction, using standard non-dimensional parameters. The Prandtl number P_r is a property of the working fluid and the Reynolds number R_e is the property of flow. Their mathematical expressions are given below.

$$Re = \frac{\dot{m}_0 d_h}{\mu} \tag{16}$$

$$\mathrm{Pr} = \frac{C_p \mu}{k} \tag{17}$$

Where μ is the dynamic viscosity of the gas, $\dot{m}_0$ is the mass flow rate per unit area, k is the thermal conductivity of the gas, C_p the specific heat of the gas and d_h is the hydraulic diameter of the regenerator matrix.

The Stanton number S_t relates the heat transfer coefficient h, the specific heat c_p, density ρ, and flow velocity u of the flow, as follows:

$$S_t = \frac{h}{C_p \rho u} \tag{18}$$

To determine the heat transfer coefficient we need to know the correlation between Prandtl, Reynolds and Stanton number. Different correlations of the form:

$$St * Pr = c\ Re^{-n} \tag{19}$$

are provided for different matrices having different characteristics (porosity, pitch and wire diameter) in Kays and London [32]. The constants *c* and *n* depends on the type of matrix geometry. Therefore, once the Reynolds number is known, the product *St*Pr* is read from the graph in [32]. Using the value of Prandtl number from eq. (17) the Stanton number can be obtained. Then the heat transfer coefficient is determined from eq. (18).

The effectiveness of the regenerator can also be determined using the effectiveness-Number of Transfer Units (ε-NTU) method. NTU is used to measure the rate of heat transfer in heat exchangers, and is a function of the type of heat exchanger and its physical size. From the definition of regenerator effectiveness eq. (10), it is the ratio of actual heat transferred to/from the regenerator from/to the fluid to the maximum possible heat transfer. That is:

$$\varepsilon = \frac{\dot{q}_{actual}}{\dot{q}_{max}} \tag{20}$$

The actual heat transfer is:

$$\dot{q}_{actual} = C_h\left(T_{h,i} - T_{h,o}\right) = C_c\left(T_{c,o} - T_{c,i}\right) \tag{21}$$

The maximum possible heat transfer in regenerator occurs when the gas is heated from cold gas inlet temperature to the regenerator $T_{c,i}$ to the temperature $T_{h,i}$ of hot gas entering the regenerator from the heater space, or vise versa. Therefore, it is given by:

$$\dot{q}_{max} = C_{min}(T_{h,i} - T_{c,i}) \tag{22}$$

Where, $C_{min} = min(C_c, C_h)$ (23)

C_h - the heat capacity of the hot gas

C_c - the heat capacity of the cold gas

The use of C_{min} instead of C_{max} in eq. 22 is due to the fact that maximum heat transfer is attained when the fluid with smaller heat capacity rate (or the smaller mass flow rate when both fluids have the same specific heat value) experiences the maximum temperature change. In the present analysis the hot gas heat capacity and cold gas heat capacity are assumed to be equal. Hence:

$$C_{min} = C_c = C_h = C_{gas} = \dot{m}\, c_P \quad (24)$$

The regenerator heat capacity matrix is given by:

$$C_{matrix} = \frac{m_m c_{P,m}}{\lambda} \quad (25)$$

Where $c_{P,m}$ is the regenerator heat capacity ratio, and λ is the fluid flow period for one complete cycle.

The matrix heat capacity ratio C_r, which is a measure of the thermal capacity of the matrix relative to the minimum flow stream capacity, is given by:

$$C_r = \frac{C_{matrix}}{C_{min}} \quad (26)$$

The larger the matrix capacity ratio, the smaller is the matrix temperature swing and, in general, the more efficient the regenerator [30].

The fluid heat capacity ratio C measures the thermal imbalance of the flow streams. It is given by:

$$C = \frac{C_{min}}{C_{max}} \quad (27)$$

Now, to determine the NTU of the regenerator we need to find the modified overall heat transfer coefficient, U_0. We consider the heat transfer coefficient of the regenerator material is unchanged during the hot and cold gas flow, i.e. $h_h = h_c = h$. It is calculated from:

$$\frac{1}{U_0 A} = \frac{1}{A h_h} + \frac{1}{A h_c} \quad (28)$$

$$U_0 A = \frac{Ah}{2} \tag{29}$$

The NTU of the regenerator is determined from eq. 30 as:

$$NTU_0 = \frac{AU_0}{C_{min}} \tag{30}$$

From eq. 30, for a given value of U_0 and C_{min} the NTU_0 is directly proportional to the heat transfer area A. Hence, NTU_0 is a measure of the heat transfer area; and the larger the NTU_0, the larger the heat exchanger (regenerator).

Once the NTU_0 is known, the effectiveness of the regenerator is determined from the following equation:

$$\varepsilon_r = \frac{NTU_0}{1+ NTU_0} \tag{31}$$

With the introduction of two characteristic dimensionless parameters, the effectiveness of a regenerator can also be read from graphs, such as the one shown in Fig. 10. The two dimensionless parameters are the reduced length Λ and reduced period Π. Λ has the similar definition as *NTU*, and designates the thermal size of the regenerator. The Λ-Π method for finding the effectiveness is primarily used for the design of fixed-matrix regenerators. They are given as:

$$\Lambda = 2NTU_0 \tag{32}$$

$$\Pi = \frac{2NTU_0}{C_r/C_{min}} \tag{33}$$

The ratio Λ/Π is called a utilization factor, and it is the ratio of the heat capacity of the working fluid for the blow period to the heat storage capacity of the matrix.

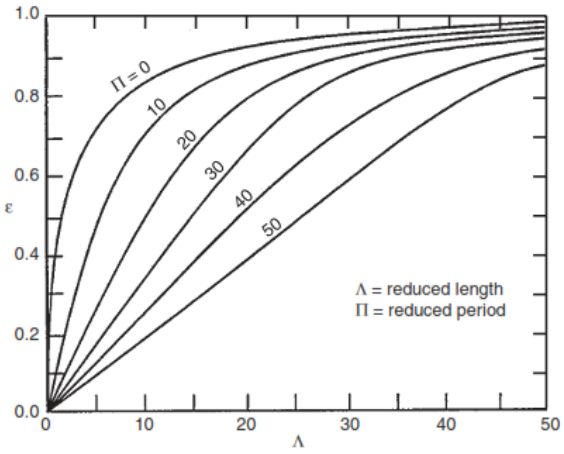

Fig. 10. Effectiveness chart for a balanced and symmetric counter flow regenerator [33].

Substituting eq.22 and eq.31 into eq.20, the actual heat transfer to/from the regenerator can be estimated as:

$$\dot{q}_{actual} = \varepsilon_r \dot{q}_{max} = \varepsilon_r \dot{m} c_{P,gas} \left(T_{h,i} - T_{c,i}\right) \quad (34)$$

3.12. Regenerator matrix surface selection

Six different screen matrix surfaces were studied to select the best wire mesh screen to be used as a regenerator for the Stirling engine. The geometrical dimensions as well as other important specifications of the screen matrices are given in Kays and London [32]. The input parameters used for the performance analysis of all the different regenerator screen matrices are the same. The input values are given in Table 1. Stainless steel Grade-316 is used for the screen materials.

For each screen surfaces the NTU, effectiveness, pressure loss, fluid mean velocity, fluid mass flow rate and the ratio of heat transfer area to pressure loss are calculated. The calculation is presented in Table 2.

In the regenerator screen surface selection analysis, the mass flow rate of the gas is constant since the density of gas, swept volume and speed of the piston are constant. In addition, volume and length of regenerator are also fixed for all the cases.

Table 1. Input parameters for regenerator material

Parameter	Value	Unit
Working fluid	Helium	
Regenerator volume	0.005	m^3
Engine Speed	750	Rpm
Swept volume	0.0053	m^3
Regenerator length	0.1	m^3
Reg. material density	8000	kg/m^3
Reg. Sp. Heat capacity	502	J/kg-K

The mesh size (or mesh density) of a given screen is determined by the wire diameter. For a given screen size, increase in wire diameter decreases the porosity since the volume occupied by the wire material increases but this introduce high friction loss. In addition, for a given constant number of screens, increase in wire diameter increases the length of the regenerator. On the other hand, increasing wire diameter increases the mass of the regenerator which in turn improves the heat capacity of the regenerator. But reducing wire diameter for a given screen size increases the porosity which in turn increases the heat transfer surface area at a cost of reduced heat capacity.

Table 2. Results of the study made on the performance of different screen matrix surfaces available in Kays and London [32].

	Screen matrix surfaces					
	60x60x0.0075	60x60x0.011	24x24x0.014	16x16x0.018	10x10x0.025	5x5x0.041
Wire diameter, mm	0.1930	0.2667	0.3429	0.4445	0.6223	1.0414
Mesh per inch	58x61	55x60	$24x24\frac{1}{4}$	$16\frac{1}{4}x16\frac{1}{8}$	10x10	$5\frac{1}{8}x5\frac{1}{16}$
Screen thickness, mm	0.432	0.724	0.648	0.851	1.35	2.01
Porosity	0.675	0.602	0.725	0.766	0.817	0.832
Hydraulic diameter, mm	0.394	0.405	0.902	1.50	2.83	5.18
Heat transfer surface area, m^2	50.55	49.58	21.33	13.75	7.20	3.88
Free flow area, m^2	0.03375	0.0301	0.03625	0.0383	0.04085	0.0416
Regenerator diameter, m	0.252	0.252	0.252	0.252	0.252	0.252
NTU	211.55	182.93	78.94	44.93	19.92	8.42
Effectiveness	0.995	0.995	0.987	0.978	0.952	0.894
Mass flow rate, kg/s	0.022	0.022	0.022	0.022	0.022	0.022
Fluid mean velocity, m/s	3.926	4.402	3.655	3.460	3.244	3.185
Coefficient of friction	3.5	4	1.5	1.3	1.1	0.75
Pressure loss, Pa	1139.72	1593.20	184.81	172.64	34.04	12.22
Power loss, W	9060.77	12665.9	1469.23	1372.52	270.62	97.13
Mass of matrix, kg	13	15.92	11	9.36	7.32	6.72
Heat transfer area to pressure loss ratio, m/Pa	0.044353	0.03112	0.11542	0.07965	0.21152	0.3175

The selection of best screen matrix among the considered mesh geometries requires a tradeoff between different factors. The heat transfer area to pressure loss ratio is considered as the best screen surface selection criteria [31]. Based on this, regenerator with screen matrix surface of 5x5x0.041 (right most column in Table 2) is selected for the Stirling engine under study.

3.13. Stirling engine thermodynamics analysis

The Stirling engine studied in this report is modeled based on the first order analysis (Schmidt analysis). The thermodynamics analysis of the cycle is performed in EES environment [33]. Results from the analysis are presented and discussed.

The following assumptions are made to simplify the analysis:

- ✓ The cycle is under steady state condition.
- ✓ The working gas obeys perfect gas law: $PV=mRT$
- ✓ The mass of the working gas is constant and there is no leakage.
- ✓ Volume variation in the working spaces is sinusoidal.
- ✓ The temperatures in the cold space, hot space and regenerator are isothermal at T_C, T_H and T_R respectively.
- ✓ Pressure is constant in each space.
- ✓ Alpha type engine configuration is considered
- ✓ To resemble a real Stirling engine, the dead volumes of the regenerator, hot and cold spaces are taken into account in the analysis.

The equations used for the analysis of the Stirling engine under the isothermal assumption and including the dead volumes of the regenerator, hot and cold spaces are summarized below. Detail analysis can be found in [1].

Total dead volume V_S is the sum of the hot, regenerator and cold space dead volumes, V_{SH}, V_{SR} and V_{SC} respectively:

$$V_S = V_{SH} + V_{SR} + V_{SC} = (k_{SH} + k_{SR} + k_{SC})V_S \quad (35)$$

Where: $k_{SH} = V_{SH}/V_S$ is the hot space dead volume ratio,

$k_{SR} = V_{SR}/V_S$ is the regenerator space dead volume ratio,

$k_{SC} = V_{SC}/V_S$ is the cold space dead volume ratio

Regenerator effectiveness:

$$e = (T_{3'} - T_1)/(T_3 - T_1) \quad (36)$$

Regenerator effective temperature:

$$T_R = (T_{3'}+T_{1'})/2 = (T_3+T_1)/2 \quad (37)$$

Total mass of the working fluid is the sum of masses contained in each space:

$$m = m_H + m_{SH} + m_R + m_C + m_{SC} \quad (38)$$

Instantaneous system pressure:

$$p = mR / (V_H/T_3 + K + V_C/T_1) \quad (39)$$

where: $K = V_{SH}/T_3 + V_{SR}/T_R + V_{SC}/T_1$ (40)

Mean pressure:

$$p_m=(mR/V_P)\{T_3 \ln[(V_D+V_P+KT_3)/(V_D+KT_3)] - T_1 \ln[(V_D+V_P+KT_1)/(V_D+KT_1)]\} \quad (41)$$

Total heat input:

$$Q_{in}=mC_V\{(1-e)(T_3-T_1)+(k-1)T_3*\ln[(V_D+V_P+KT_3)/(V_D+KT_3)] \quad (42)$$

Where: k is the specific heat ratio

Total heat rejected:

$$Q_{in}= -mC_V\{(1-e)(T_3-T_1)+(k-1)T_1* \ln[(V_D+V_P+KT_1)/(V_D+KT_1)] \quad (43)$$

Net work output:

$$W_{net}=mR\{T_3 ln[(V_D+V_P+KT_3)/(V_D+KT_3)]-T_1 ln[(V_D+V_P+KT_1)/(V_D+KT_1)]\} \quad (44)$$

Thermal efficieny: $\eta_{th}=W_{net}/Q_{in}$ (45)

Carnot efficiency: $\eta_{carnot}=1 - T_1/T_3$ (46)

3.14. Results and discussion

The performance of the Stirling engine is evaluated and the results are presented in this section. The input values used for the analysis are given in Table 3. Results of the analysis at the input values are also presented. The effect of varying the effectiveness of the regenerator, hot temperature and phase angle on the cycle efficiency, heat input and net work output are studied and the results are given in Figs. 11 to 17.

Table 3. Input values of the Stirling engine analysis.

Parameters	Unit	Value
Working gas		Helium
Hot temperature, T_H	K	523
Cold temperature, T_C	K	353
Regenerator effectiveness, e		0.894
Compression ratio, CR		1.5
Engine speed, n	rpm	750
Phase angle, ϕ	Degree	90

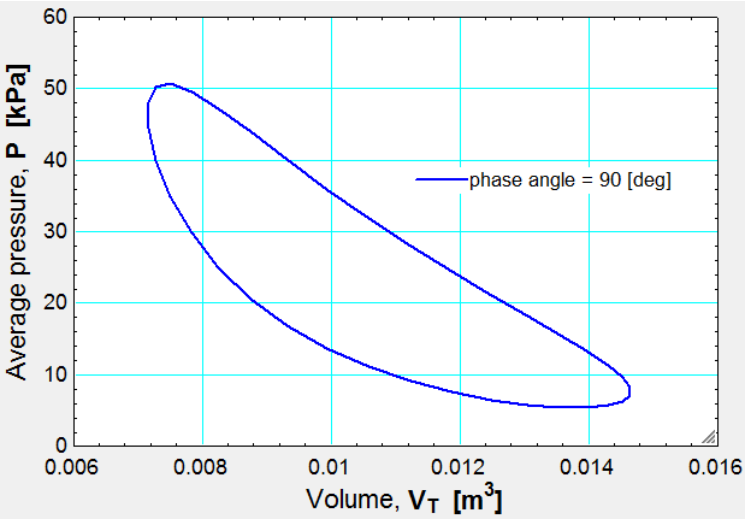

Fig. 11. P-V diagram of the modeled Stirling engine.

Fig. 11 shows the P-V diagram of the Stirling cycle engine at phase angle of 90^0. This is way different from the theoretical Stirling cycle P-V diagram in Fig. 2, although does not correspond yet to the actual diagram.

The results of the computation at the input values are given below:

Unit Settings: SI K kPa kJ mass deg

$a = 55.98$ [deg]	$B = 1.206$ [-]	$c = 0.4145$ [-]
$CR = 1.5$ [-]	$C_v = 3.116$ [kJ/kg-K]	$e = 0.894$ [-]
$\eta_{carnot} = 0.325$	$\eta_{ratio} = 0.6212$	$\eta_{th} = 0.2019$
F$ = 'Helium'	$K = 0.000009275$ [m^3/K]	$KT_1 = 0.003274$ [m^3]
$KT_3 = 0.004851$ [m^3]	$k_{SC} = 0.2$ [-]	$k_{SDP} = 0.3774$ [-]
$k_{SH} = 0.2$ [-]	$k_{SR} = 0.6$ [-]	$k_{ST} = 0.274$ [-]
$m = 0.001703$ [kg]	$n = 750$ [revs/minute]	$P = 46.42$ [kPa]
$\phi = 90$ [deg]	Power $= 2.202$ [kW]	$P_{mean} = 33.24$ [kPa]
$Q_{11} = -0.09559$ [kJ]	$Q_{12} = -0.6007$ [kJ]	$Q_{23} = 0.9018$ [kJ]
$Q_{2r} = 0.8062$ [kJ]	$Q_{33} = 0.09559$ [kJ]	$Q_{34} = 0.7769$ [kJ]
$Q_{41} = -0.9018$ [kJ]	$Q_{4r} = -0.8062$ [kJ]	$Q_{in} = 0.8725$ [kJ]
$Q_{out} = -0.6963$ [kJ]	$R = 2.077$ [kJ/kg-K]	$S = 2.911$ [-]
$t = 0.675$ [-]	$\theta = 45$ [deg]	$T_R = 438$ [K]
$v = 1$ [-]	$V_C = 0.001576$ [m^3]	$V_{C1} = 0.0106$ [m^3]
$V_{C2} = 0.0053$ [m^3]	$V_D = 0.0053$ [m^3]	$V_H = 0.001576$ [m^3]
$V_P = 0.0053$ [m^3]	$V_R = 0.0024$ [m^3]	$V_S = 0.004$ [m^3]
$V_{SC} = 0.0008$ [m^3]	$V_{SH} = 0.0008$ [m^3]	$V_{SW} = 0.0106$ [m^3]
$V_T = 0.007152$ [m^3]	$W_{12} = -0.6007$ [kJ]	$W_{34} = 0.7769$ [kJ]
$W_C = -0.0672$ [kJ]	$W_E = 0.09956$ [kJ]	$W_{net} = 0.1762$ [kJ]
$W_T = 0.03236$ [kJ]	$X_{DC} = 0.1509$ [-]	$X_{DE} = 0.1509$ [-]
$X_R = 0.4528$ [-]		

3.14.1. Effect of regenerator effectiveness

The thermal efficiency and heat transfers at the cooler, heater and regenerator are dependent on the effectiveness of the regenerator. But, the regenerator effectiveness has no effect on the output work and the maximum power output [1, 35]. Regenerator with high effectiveness value improved the cycle efficiency and reduced the required heat input, Figs. 12 and 13, respectively. An increase in effectiveness from 0.8 to 0.9 increases the cycle efficiency from 18.3% to 20.1% and reduced the total heat input from 0.96 kJ to 0.88 kJ. This is expected because the thermal efficiency is inversely related to the heat input; and

regenerator with high effectiveness value is capable of storing and releasing large amount of heat therefore reducing the required external heat input.

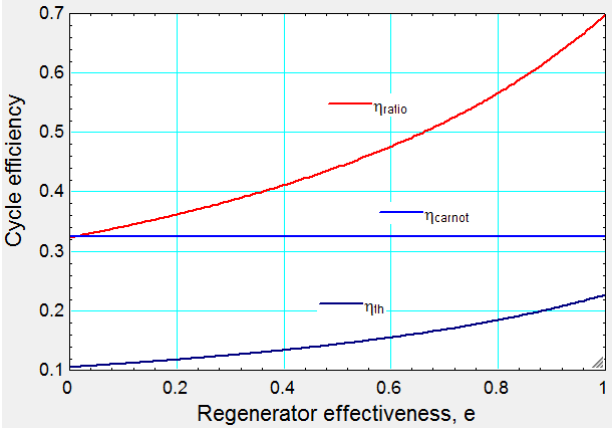

Fig. 12. Effect of regenerator effectiveness on cycle efficiency.

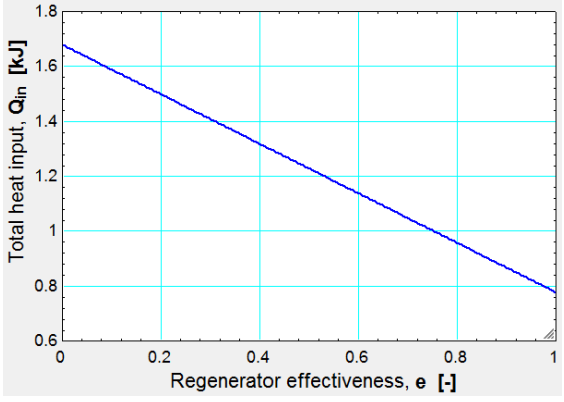

Fig. 13. Effect of regenerator effectiveness on total heat input.

3.14.2. Effect of hot temperature

Figs. 14 to 16 illustrate the effect of hot temperature on the cycle efficiency, total heat input and net work output. The efficiency, heat input and new work

output of the cycle increased with increasing hot temperature. As can be seen in the theoretical T-S diagram of Stirling engine in Fig. 3, line 3-4 is in isothermal heat addition process and the area under this line is the heat input. Therefore, increasing the hot temperature increase the area under the isothermal heat addition line (process 3-4) (Fig. 14(b)). The cold temperature was fixed at T_C=353K, therefore the area under process 1-2 has not changed during this process. The net work output is the difference of the areas under process 3-4 and process 1-2. Therefore, increasing the hot temperature increases the net work output (Fig. 16)

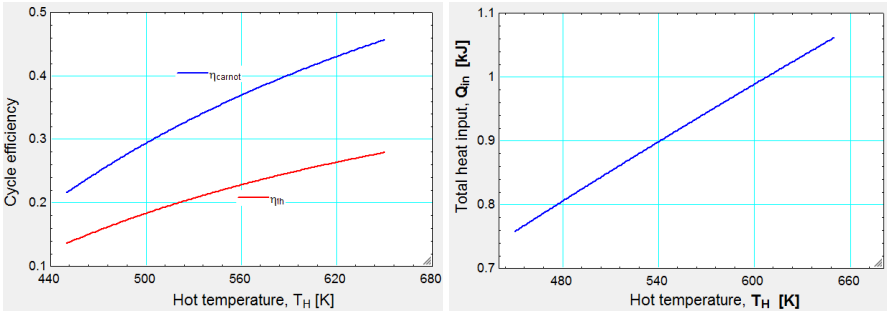

(a) (b)

Fig. 14. Effect of hot temperature on: (a) cycle efficiency; (b) heat input.

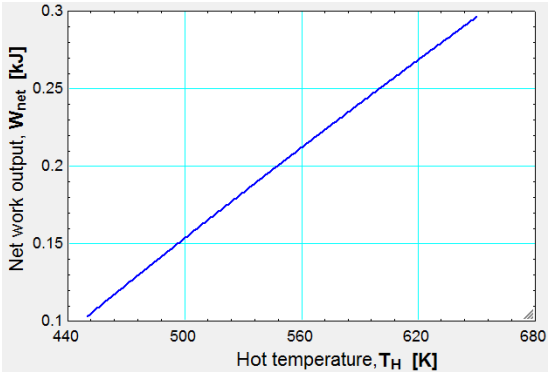

Fig. 16. Effect of hot temperature on net work output.

In general, increasing the hot temperature increases the net work output and thermal efficiency of the engine but the highest temperature is limited by the induced thermal stress that the material can resist [35].

3.14.3. Effect of phase angle

Fig. 17 presents the effect of changing the phase angle between power and displacer pistons. It is observed that increasing the phase angle reduced both the heat input and net work output. But the cycle efficiency did not change. Increasing the phase angle has a positive advantage in reducing the required heat input at the cost of reducing the net work output. Therefore, an optimal phase angle should be used in designing a Stirling engine. In the present study a phase angle of 90^0 is used. A phase angle of 90^0 is suggested as optimal [21] for a Stirling engine.

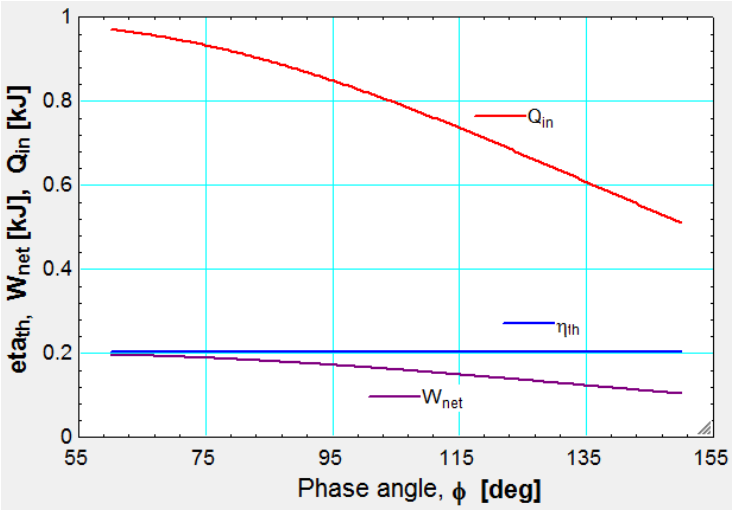

Fig. 17. Effect of phase angle on the performance of Stirling engine.

4. The Organic Rankine Cycle (ORC)

The ORC is derivative of the Rankine cycle that uses organic working fluids instead of steam as in steam Rankine cycle. The four main components (turbine, condenser, pump and boiler) of the ORC are shown in Fig. 18.

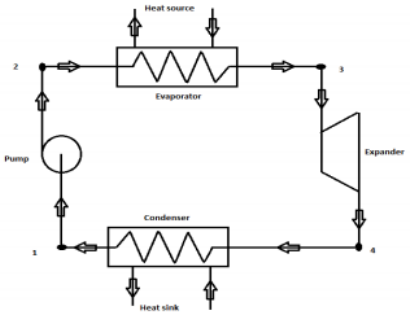

Fig.18. Basic layout of an ORC.

4.1. Application areas

The organic Rankine cycle is the widely used thermodynamic cycle for low-grade heat conversion. It can efficiently be used in many applications to produce electrical power or mechanical work. The following are some of the application areas.

Solar thermal power

In recent years the ORC technology is getting wider acceptance for converting solar energy in to electricity. Many researchers have studied the feasibility of coupling ORC with solar thermal for power production [7, 36, 37]. ORC can be coupled with parabolic through, solar tower or parabolic dish to harness the solar energy to heat water or other working fluids, which deliver the required heat input for the ORC. It is an attractive technology for small distributed power generation in remote areas compared to the fossil fuels power generation.

Waste heat

The use of organic working fluid with low boiling point in Rankine cycle makes it efficient to convert the low-grade heat that is coming out of different industrial processes in to electricity. Some of the sources of waste heat are hot exhausts from ovens or furnaces (e.g. lime and cement kilns), flue-gas condensation, exhaust gases from vehicles, intercooling of a compressor, condenser of power cycle, etc. Studies are being made to utilize this technology for power generation [38].

Geothermal

There are abundant geothermal resources available in different part of the world. These sources provide heat in the temperature range of 50 to 350^0C, and can either be dry, mainly steam, a mixture of steam and water, or just liquid water. The conversion technologies required to extract the heat are determined by the available temperature of the resource [9, 39].

High temperature reservoirs with temperature above 220^0C are commercially viable for electricity production [39]. The most commonly available geothermal sources have temperature in the range of 100 – 220^0C. ORC is an efficient technology for converting heat to electricity.

4.2. Organic fluid classification

The organic fluids used for ORC are generally classified in to three groups based on the slope (*dT/ds*) of saturated vapor curve in a T-s diagram [8], see Fig. 19. Fluids having positive slope are classified under "dry" fluids, and they usually have higher molecular mass (*M*), e.g. HFE7000 *M* = 200 and HFE7100 *M* = 250. Fluids with negative slope on the saturated vapor curve are grouped under "wet" fluids. These fluids are commonly of low molecular mass, such as water *M* = 18 and ammonia *M* = 17. The third category of fluids which have nearly vertical saturated vapor curves are called "isentropic" fluids. These are

generally of medium molecular mass, such as R134a M = 102, R245fa M = 134 and R123 M = 153.

Since for isentropic fluids the value of dT/ds leads to infinity, the inverse of the slope, (i.e. ds/dT) is used to express how ‘‘dry’’ or ‘‘wet’’ a fluid is.

For “wet” fluids, due to the negative slope of the saturated vapor curve on T-s diagram, there is formation of liquid droplet at the end of expansion. Formation of liquid in a turbine may damage turbine blades. A dryness fraction of below 85% will significantly reduce the isentropic efficiency of the turbine [13]. As a result super heating of the fluid is required before entering the turbine. But as the vapor is superheated there is reduction in heat transfer coefficient, accordingly the heat transfer area required increases and this boost the cost of the superheater [13].

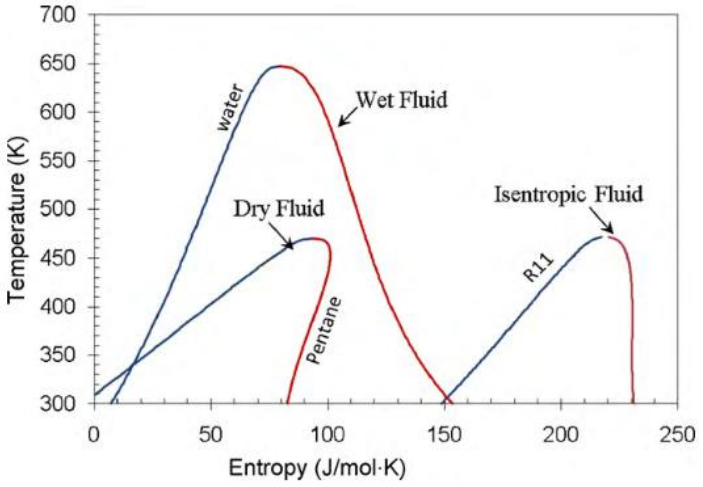

Fig. 19. Three categories of fluids: dry, isentropic and wet [40].

“Dry” and “isentropic” fluids appear to be solutions to the problem of liquid formation during expansion of “wet” fluids. In addition, there is no need for superheating the fluid entering the turbine. To avoid liquid formation during the expansion process in the turbine “dry” and “isentropic” fluids are recommended

for ORC application [8, 41, 42]. The drawback of "too dry" fluids is the requirement of high cooling load at the condenser as they will leave the expansion unit with substantial superheat. But this can be overcome by the use of internal heat exchanger or a regenerator, where the superheat vapor at the turbine exit can be used to preheat the fluid exiting the feed pump before entering the evaporator. This internal heat exchange increases the cycle efficiency at the cost of systems initial investment and complexity [13]. During expansion, isentropic fluids expand along the nearly vertical line of the saturation vapor curve hence the fluid leaving the expander is saturated vapor. Therefore, the load on the condenser is low compared to condensation of "dry" fluids, and there is no need to install regenerator. In the present study, only "dry" and "isentropic" organic fluids are considered.

4.3. Working fluid properties and selection criteria

The performance of an ORC depends primarily on the working fluid, available heat source and heat sink, and system component performance. The working fluids must have not only thermodynamic properties that match the application but also adequate chemical stability at the desired working temperature and pressure, environmentally friendly, and economical viability.

Selection of appropriate working fluid and of the particular cycle design with which the optimum objective function can be achieved are the main challenges associated with the ORC technology. Several comparisons among different organic fluids for ORC have been conducted and can be found in references [6, 11, 43, 44, 45]. These comparisons were made under certain predefined operating condition (temperature) and few fluids are used. However, fluid(s) suggested as best working fluid and cycle with highest efficiencies may not hold true under other working conditions and among other working fluids.

Different criteria are used for the selection of organic working fluid for ORC applications. Several researchers [12, 40, 43, 46] have set out different selection

criteria based on the specific working condition of the ORC system. These fluid properties and selection criteria, as given in [40], are discussed below.

Vaporization latent heat: organic fluids with higher latent heat of vaporization enable most of the available heat to be added during phase change operation; and this, in addition to avoiding the need to superheat the fluid; it also leads to small equipments at the pump, evaporator and condenser level [11, 47].

Density: fluid volume flow rate at the exit of the expander determines the size of the expander, which has a significant impact on the system cost. High vapor density leads to a lower volume flow rate, hence small size expander and condenser. Angelino et. al. [48] suggest that the ratio of the density of vapor across the expander (i.e. ρ_{in}/ρ_{out}) should be lower than 50 to achieve a turbine efficiency higher than 80%.

Specific heat: The C_p of fluid in liquid phase should be small, namely the curve of saturation in liquid phase should be as vertical as possible. Even though, there is no direct relationship between specific heat and pump work, researchers suggest that low specific heat could decrease the work consumed by pump and increase the work output [13, 40].

Critical temperature: in almost all ORC's designs condensation temperature is normally above 300K in order to reject heat to the ambient. Therefore, the working fluids must have critical temperature far above the condensation temperature [40]. For supercritical ORC the working fluid critical temperature must be below the condensation temperature.

Boiling temperature: for safety reasons working fluids can be easy to handle at ambient environment, so the boiling temperature is expected to be $0 - 100^0$C [6, 40].

Freezing point: the lowest temperature of the ORC must be higher than the freezing point of the fluid.

Molecular weight: high molecular weight has a positive impact on turbine efficiency. It also slows down the flow rate. However, fluids with high critical pressure and high molecular weight require higher heat transfer area.

Viscosity: this is important especially in the heat exchangers, because low viscosity both in liquid and vapor phases maintain low friction losses.

Conductivity: to achieve high heat transfer coefficient in the heat exchangers, fluids with high conductivity are preferred.

For the present study, considering the criteria mentioned above six fluids were selected and studied under the same working condition. Three of the working fluids are "isentropic" fluids while the other three are "dry" fluids. Properties of the selected fluids are given in Table 4.

Table 4: Properties of organic fluids analyzed in this study

Fluid	Molecular Formula	Molecular mass (kg/kmol)	P_{crit} (MPa)	T_{crit} (K)	T_{bp} (K)	ATL (yr)	ODP	GWP (100yr)
R123[i]	$C_2HCl_2F_3$	152.93	3.67	456.85	300.95	1.3	0.012	77
R134a[i]	$C_2H_2F_4$	102.03	4.06	374.18	247.08	14	0	1430
R600a[i]	C_4H_{10}	58.12	6.64	407.85	261.41	0.019	0	~ 20
R245fa[d]	$C_3H_3F_5$	134.05	3.64	427.21	288.29	8.8	0	820
R600[d]	C_4H_{10}	58.12	3.80	425.15	272.63	0.018	0	~ 20
n-Pentane[d]	C_5H_{12}	72.15	3.39	460.35	300.95	0.01	0	~ 20

4.4. Solar ORC System description

The overall system configuration of the solar powered ORC system, shown in Fig. 20, is adopted from [43] and used in the present study. It can be divided into two sub-systems: the solar energy collector system and the ORC system.

The solar energy collector system is a closed circuit system composed of a flat plate collector, a thermal storage tank and a water pump. Water is heated up while passing through the collector field and driven to the thermal storage tank, where it stores and transfers the heat collected from the sun to the working fluid of the ORC in the evaporator. Then returns back to the thermal storage tank

where it is pumped again to the collector field. Transferring the heat from the sun directly to the evaporator of the ORC system will result in fluctuation of the temperature of the working fluid entering the expander. Therefore, use of thermal storage tank guarantees best control and regulation of cycle performance [43].

The second sub-system is the ORC unit. The ORC unit has the four main components (turbine, condenser, pump and evaporator) and a preheater. The preheater heats the working fluid before entering the evaporator using heat from the heat source. Preheating the fluid before entering the evaporator, have a significant improvement on the system efficiency.

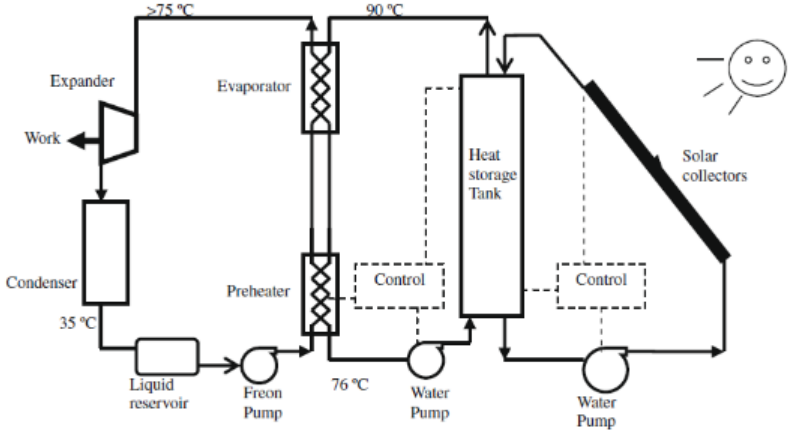

Fig. 20. Layout of solar powered ORC used in the present study, modeled by [43].

The overall system is designed to provide a net electrical power output of 2 kW for a residential building application. To reduce the overall cost of the system a good quality flat plate collector is employed to harness the solar energy. It has total collector area of 600 square meters and has no tracking system.

4.5. Solar ORC system modeling

The solar collector system and the ORC unit are modeled separately. To determine the required heat source temperature and heat input to meet the

targeted 2 kW power output from the ORC system, thermodynamic analysis of the ORC is performed in EES first. Then the solar collector system is modeled using Polysun software [49] to meet the temperature and heat input requirements of the ORC.

4.5.1. ORC modeling

The ORC system in this study consists of a condenser, pump, preheater, evaporator and expander. It is designed for a 2 kW power output, and is assumed to operate only during the day time for 8 hours when the solar radiation is high, i.e. from 9 am to 5 pm. Operation of the ORC at night or when there is low/no solar radiation requires a heat storage tank. But, as stated later in section 3.5.2, significant amount of heat losses through the heat storage tank and pipes makes the solar ORC system unfeasible to be operated using stored heat. In addition, operating in part-load condition might reduce the performance of the ORC.

The cycle is modeled in EES environment [33]. Each of the state point thermodynamic properties is determined and the performance of the cycle is evaluated. The performance of the ORC is evaluated based on the first and second law of thermodynamics for different organic working fluids. It is assumed that the pressure drop in each component is neglected. The first and second laws of thermodynamics are applied for each component to estimate the heat added or removed, work input or output and system irreversibility.

To simplify the analysis of the ORC the following assumptions are employed.

- ✓ The system is under steady state condition
- ✓ No pressure drops in connecting pipes and heat exchanger
- ✓ The ambient temperature is 25 ^{0}C.
- ✓ The exit temperature of the heat source stream after the evaporator is equal to the inlet temperature to the preheater.
- ✓ Heat losses in each component are ignored.

- ✓ Working fluid entering the expander is saturated vapor.

The thermodynamic equations used to measure individual component performance and cycle efficiency are summarized below.

Pump**:**

work input $\dot{W}_p = \dot{m}_{ORC}(h_5 - h_4)/\eta_p$ (47)

exergy $\dot{I}_p = T_0 \dot{m}_{ORC}(s_5 - s_4)$ (48)

Preheater:

heat added $\dot{Q}_{pre} = \dot{m}_{ORC}(h_6 - h_5)$ (49)

exergy $\dot{I}_{pre} = T_0 \dot{m}_{ORC}[(s_6 - s_5) - (h_6 - h_5)/T_{mid}]$ (50)

T_{mid} is the midpoint temperature of the heat source between the evaporator and preheater which is determined by pinch point analysis.

Evaporator:

heat added $\dot{Q}_e = \dot{m}_{ORC}(h_2 - h_1)$ (51)

exergy $\dot{I}_e = T_0 \dot{m}_{ORC}[(s_2 - s_1) - (h_2 - h_1)/T_H]$ (52)

Expander:

work output $\dot{W}_t = \dot{m}_{ORC}(h_3 - h_2) * \eta_p$ (53)

exergy $\dot{I}_t = T_0 \dot{m}_{ORC}(s_3 - s_2)$ (54)

volume expansion ratio: $VER = \frac{v_3}{v_2}$ (55)

Condenser:

heat removed $\dot{Q}_c = \dot{m}_{ORC}(h_4 - h_3)$ (56)

exergy $\dot{I}_c = T_0 \dot{m}_{ORC}[(s_4 - s_3) - \frac{(h_4 - h_3)}{T_C}]$ (57)

Total exergy destruction rate:

$$\dot{I}_{tot} = \dot{I}_p + \dot{I}_{pre} + \dot{I}_e + \dot{I}_t + \dot{I}_c \quad (58)$$

Total heat input: $\dot{Q}_{in} = \dot{Q}_e + \dot{Q}_{pre}$ (59)

First law efficiency: $\eta_{ORC} = \frac{\dot{W}_{net,ORC}}{\dot{Q}_{in}}$ (60)

Second law efficiency: $\eta_{II} = \frac{\eta_{ORC}}{1 - \frac{T_C}{T_H}}$ (61)

4.5.2. Solar thermal system modeling

The solar thermal system is modeled using Polysun software. Polysun is a simulation software developed by Vela Polaris [49]. It enables users effectively simulate solar-thermal, photovoltaic and geothermal systems, and generates a professional report including financial analysis. It has in-built pre-defined templates of different solar-thermal arrangement (also called variant) for different applications. Different templates can be selected for the same application. For the different variants selected, each of the components and connections of the solar system can be modified and/or simulated to make comparison and optimize the system. It has diverse in-built catalogs of commercially available solar collectors, pipes, storage tanks, pumps, inverters, etc, from where the user is allowed to choose. The user is also allowed to modify the thermo-physical properties of the commercially available components of the solar system in the catalog.

The first step in designing a solar-thermal system using Polysun is to define the site data, which includes location of the system, weather data, cold water temperature, storage room temperature, horizon and grid voltage and frequency, where the system is to be installed. The user can define the site either by

choosing from the database in the software or by manually entering the values. After defining the site, the user defines the load, means by which energy is provided, system specification. Then appropriate solar energy system configuration (variant) is chosen from the template provided. Based on the desired load chosen, the user defines, for instance, the size of the solar collector (for hot water demand) or size of building (for space heating). The last step in the wizard is to define a back up heat generator, when there is less solar radiation, which can be boiler or heat pump. After this, the selected system is simulated and the results can be displayed graphically or in tabular form for evaluation. The final result can be generated in the form of professional report.

In the present study, the solar thermal system is required to provide hot water at a constant temperature of 90^0 C at the inlet of the evaporator, and to return at 76^0 C to the storage tank. To satisfy this requirement a solar thermal system with a heat storage tank is modeled in Polysun. The purpose of the storage tank is to stabilize the temperature of the water entering the evaporator of the ORC system at the set point temperature.

The following input data were used for simulation of the system in Polysun software. The input data are defined based on the weather and need of the location selected.

1. Location selection from data base:
    - Region - Africa
    - Country - Ethiopia
    - Location(city) - Addis Ababa
    - Electric grid voltage: 230V
2. Template selection:
    - Consumers need/ load: Domestic hot water
    - Energy Provider: Solar-thermal
    - System Specification:
        - ✓ System size: residential system

- ✓ Collector/Generator field: single field
- ✓ DHW preparation method: potable water tank
- ✓ Template source: 8bb: Hot water (Solar thermal, low-flow)

3. Hot water demand:
   - ➢ Number of persons living in the building: 8
   - ➢ Temperature: 90˚C
   - ➢ Daily hot water demand: 400 liter
   - ➢ Absences: Never
4. Dimensioning of the solar-thermal system:
   - ➢ Test Standard: Europe
   - ➢ Collector: Flat-plate, good quality
   - ➢ Orientation: 0
   - ➢ Tilt angle: 10˚
   - ➢ Solar fraction: Medium
   - ➢ Recommended collector number: 300
   - ➢ Gross area: 600 square meter
   - ➢ Recommended tank volume: 2700 liter
   - ➢ Water tank: 750 gallon (2839.1 liter) US model

Diverse configuration of solar thermal system with different numbers of solar collectors and different sizes of storage tanks were considered in the analysis. But, the required set point temperatures were not attained. One of the main reasons for this was the high heat loss associated with the solar thermal system components, especially heat loss associated with the commercially available storage tanks and the pipes. Because of the significant amount of heat losses through the pipes and storage tank, it was necessary to customize (modify) the thermo-physical properties of these components. The pipes and storage tank are customized in such a way that the heat loss through them is neglected. In doing so, huge amount of heat was recovered and the simulation was repeated with

higher number of solar collector. Finally, the set point temperatures were attained.

In the final design, to meet the set point temperatures 90 ^{0}C at the inlet to the evaporator and 76 ^{0}C after the preheater, the total number of collector required is 300, which has a total gross area of 600 m^2. A new storage tank, HYBRID quattro 2000 (catalog number 1408), was selected from the catalog, and to avoid any heat loss its thermal conductivity is modified and is set to 0.0001W/m/K. Other properties of the storage tank are given in Table 5 and Table 6.

Table 5. Selected storage tank for the solar thermal system.

Catalog no.	Name	Manufacturer	Volume (lit)	Height (m)	Material	Wall thickness (mm)	Insulation thickness (mm)	Insulation
1408	HYBRID quattro 2000	Sailer Solarsysteme	2000	1.5	Steel	4	80	Polyester fleece

Table 6. Properties of storage tank insulation material

Catalog no.	Name	Density (kg/m^3)	Thermal conductivity (W/m/K)	Heat capacity (J/kg/K^2)
106	Polyethylene	940	0.41*	1900

* The actual value of the thermal conductivity of the insulation material was 0.41 W/m/K.

4.6. Results and discussion

Thermodynamic cycle analysis of the solar powered ORC is performed using different organic working fluids under the same working condition. The working conditions (input values) of the

Table 7. Operating conditions of the solar powered ORC.

Evaporating temperature, T_e	75 ^{0}C
Condensing temperature, T_c	35 ^{0}C
Ambient temperature, T_0	25 ^{0}C
Turbine efficiency, η_t	0.441
Pump efficiency, η_p	0.8

ORC are given in Table 7. This input values are similar with the input value used in [43]. The properties of the organic working fluids considered in this study are also given in Table 4. The heat source temperature, i.e. the hot water coming from the solar thermal system, is 90^0 C and the temperature deference in the evaporator between the working fluid and heat source is set constant at 15^0 C. Results of the analysis at the operating condition are summarized in Table 8. Validity of the computation is verified by comparing the results obtained in this work with the wok of [43], Table 9. As can be seen, good agreement in the thermal efficiency and mass flow rate of the working fluid was achieved.

Table 8. Performance comparison of different working fluid for T_e=*348K*, T_c=*308K* and *2kW* power output.

	$\dot{m}_{ORC}$ *(kg/s)*	η_{th} *(%)*	η_{II} *(%)*	$\dot{W}_p$ *(kW)*	Δh_{fg} *(kJ/kg)*	$\dot{I}_{total}$ *(kW)*	*VER*	$\dot{Q}_{in}$ *(kW)*	$\dot{m}_{source}$ *(kg/s)*	$\dot{V}_{source}$ *(lit/hr)*	$T_{mid,hot}$ *(K)*
R123[i]	0.234	4.460	24.91	0.0611	148.3	5.775	3.391	44.85	0.223	801.1	352.2
R134a[i]	0.302	3.711	20.72	0.475	116.1	7.253	3.876	53.9	0.496	1785	353.9
R245fa[i]	0.219	4.307	24.06	0.101	156.7	6.022	3.507	46.43	0.282	1014	352.7
R600[d]	0.117	4.241	23.68	0.150	300.6	6.152	2.961	47.16	0.279	1004	352.6
n-Pentane[d]	0.109	4.373	24.42	0.050	323.3	5.923	3.376	45.74	0.238	856	352.3
Isobutane[d]	0.134	4.075	22.76	0.231	261.1	6.461	2.885	49.08	0.338	1217	353.0

Table 9. Comparison of results of present work with Tchanche et al. work [47].

Fluid	Thermal efficiency		Mass flow rate	
	This work	[47]	This work	[47]
R123	4.460	4.457	0.2343	0.227
R134a	3.711	3.703	0.3018	0.244
R600	4.241	4.236	0.1166	0.108
R600a	4.075	4.055	0.1339	0.122

The effects of varying turbine inlet temperature and pressure on the system efficiency, exergy destruction rate, total heat input, working fluid mass flow rate and turbine exit volume flow rate are presented and discussed below.

4.6.1. Effect of turbine inlet temperature on cycle performance

In this section the effect of turbine inlet temperature variation on the system efficiency, mass flow rate, turbine exit volume flow rate and heat input is presented. For all the cases the condensation temperature and quality of fluid entering the turbine are set at $T_c=35^0C$ and $x_2=1$ respectively.

ORC system efficiency

As shown in Table 8, for the considered operating condition, the first law thermal efficiency of the ORC varies from *3.71 %* for R134a to *4.46 %* for R123. The effect of varying the turbine inlet temperature and pressure on the first and second law efficiencies are shown in Figs 21 and 22 respectively. In all the cases there is no superheating and the fluids enters the turbine as saturated vapor.

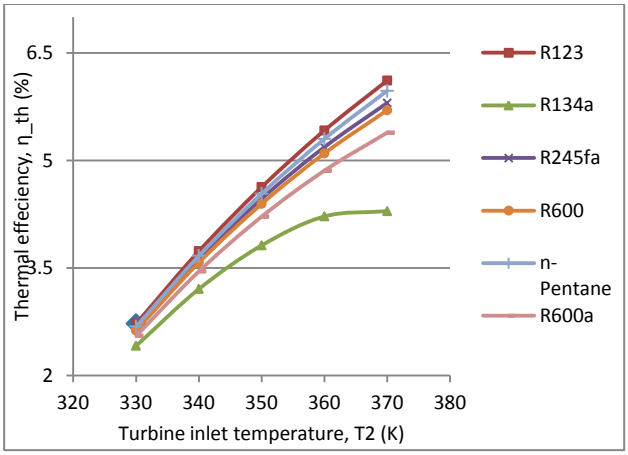

Fig. 21. Effect of turbine inlet temperature on thermal efficiency for different working fluids at $T_c=35^0C$ and $x_2=1$.

As shown in the graphs, increasing turbine inlet temperature increases the first and second law thermal efficiencies of the system for all working fluids. Looking at Table 8 and Fig. 21, fluids with higher boiling point, also critical temperature, show better efficiency at higher turbine inlet temperature. Similar observation was reported in [12], where they stated that thermal efficiencies are strong functions of the critical temperatures of the working fluids. For fluid R134a, increasing the turbine inlet temperature near its critical temperature has very low effect on the cycle thermal efficiency.

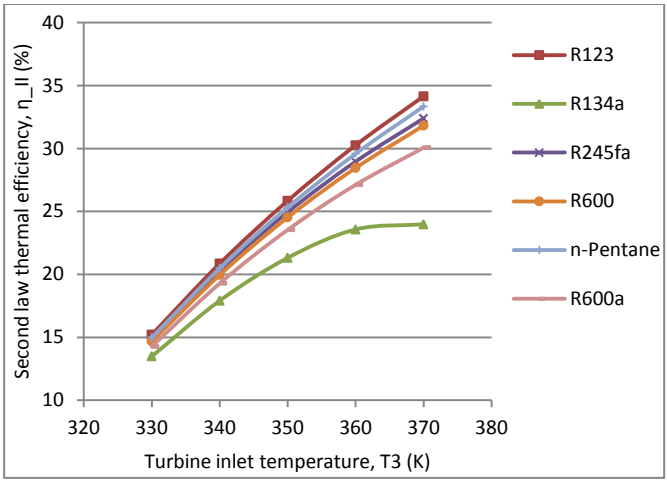

Fig. 22. Effect of turbine inlet temperature on the second law thermal efficiency for different working fluids at $T_c=35^0C$ and $x_2=1$.

Total exergy destruction rate

System irreversibility (exergy destruction rate) as a function of turbine inlet temperature is presented is presented in Fig. 23. All the fluid show reduction in exergy destruction rate as the turbine inlet temperature rises. The exergy destruction rates of R123, R600, R245fa and n-Pentane is very close to each other. Again, for R134a increasing the turbine inlet temperature near its critical temperature has very small effect on the exergy destruction rate.

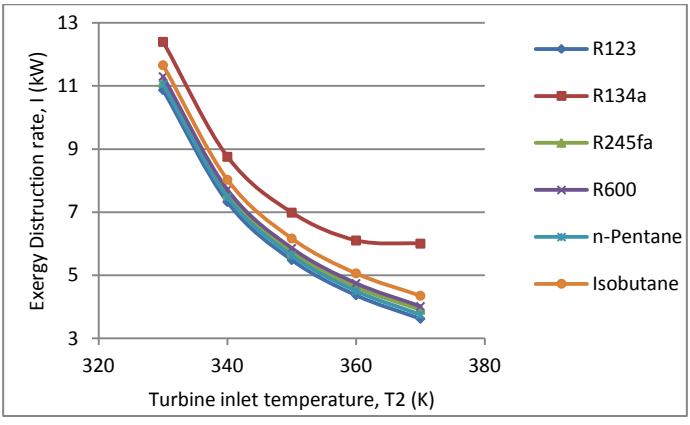

Fig. 23. Effect of turbine inlet temperature on the system exergy destruction rate, at $T_c=35^0C$ and $x_2=1$.

Mass flow rate

Fig. 24 shows the change in mass flow rate of the working fluid as a function of turbine inlet temperature. The mass flow rate of the working fluid depends on the enthalpy heat of vaporization Δh_{fg}[43]. Fluids with high enthalpy heat of vaporization require lower mass flow rate. This is observed in the present study, fluid R134a has the lowest heat of vaporization (*116.1 kJ/kg*) and highest mass flow rate (*0.302 kg/s*) while n-Pentane has the highest heat of vaporization (*323.3 kJ/kg*) and lowest mass flow rate (*0.109 kg/s*) in the range of temperatures considered and n-Pentane has the lowest.

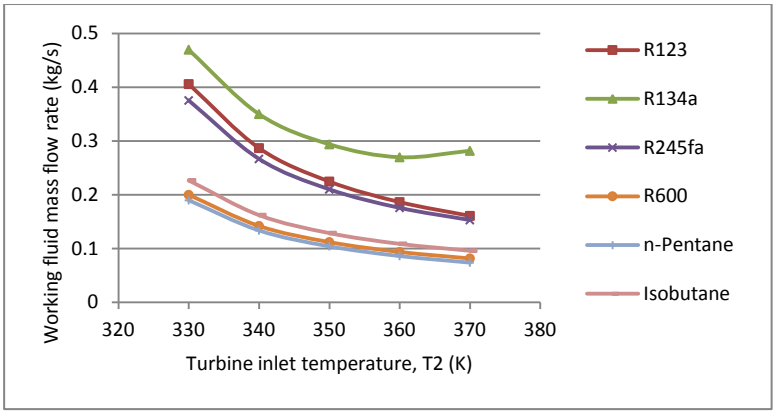

Fig. 24. Effect of turbine inlet temperature on mass flow rate.

Volume flow rate

The volume flow rate of the fluid leaving the turbine determines the size, also cost, of the turbine. Fluids with higher specific volume ratio across the turbine will lower their effectiveness [47, 50]. As shown in Fig. 25, R134a has the lowest turbine exit flow rate and n-Pentane has the highest. Considering this,

R134a has a better economical advantage, as it requires small size components [43].

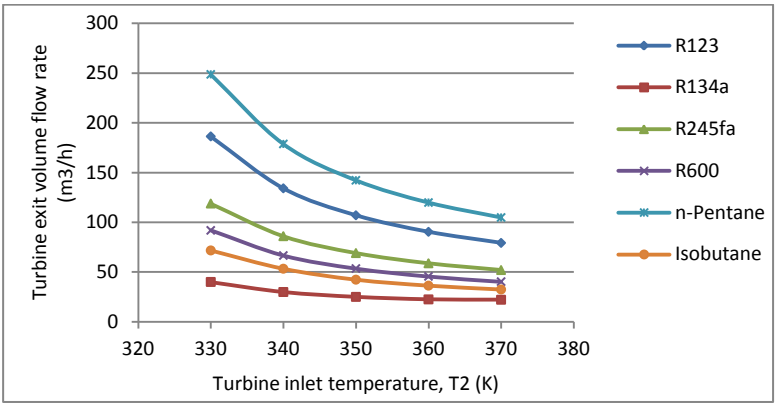

Fig. 25. Turbine exit volume as a function of turbine inlet temperature, at $T_c=35^0C$ and $x_2=1$.

Heat input rate

Study on the heat input rate, Fig. 26, shows that each of the fluids requires less heat input at higher turbine inlet temperature. The heat input determines the size of the collector array, hence the cost of the system [43]. High heat input rate is required when the ORC is operated with R134a (53.9kW) and the lowest is when it is working with R123 (44.85 kW). n-Pentane, R245fa and R600 also has low heat input rate. Observing the heat source stream flow rate in Table 8, as the heat input increases the heat source stream flow rate also increases for the different fluids considered. Low heat source flow rate requires small size pump, heat storage tank and small number of solar collectors, therefore reduces the total cost of the system. Fluid R123 has the best advantage in this regard, followed by n-Pentane, R245fa, R600 and isobutane.

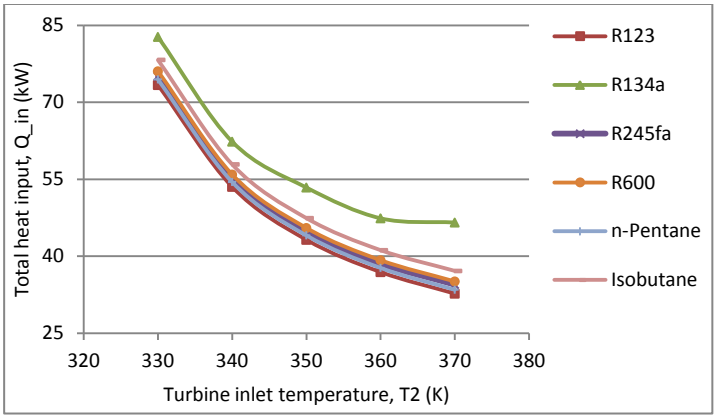

Fig. 26. Effect of turbine inlet temperature on the heat input, at $T_c=35^0C$ and $x_2=1$.

4.6.2. Effect of turbine inlet pressure on system performance

Thermal efficiency

For all fluids, unlike temperature, increase in turbine inlet pressure has a negative effect on the ORC's first and second law efficiencies, as shown in Figs. 27 and 28. For each fluid, the pressure variation was made around the working pressure of the evaporator obtained based on the input values. In each case, the critical pressures of the fluids are much higher than the working pressure. R134a has the highest working pressure among the tested fluids and n-Pentane the lowest.

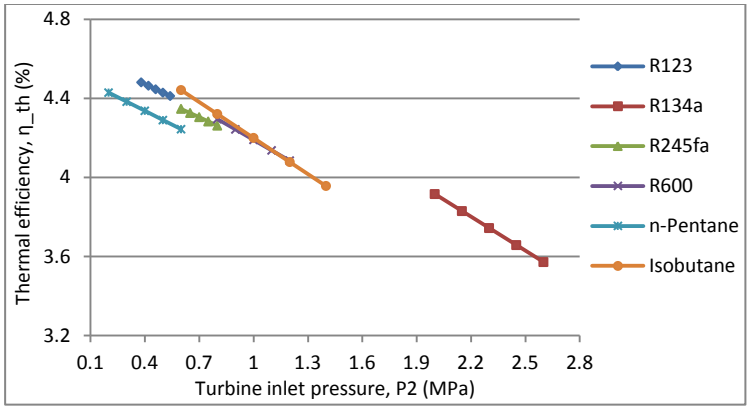

Fig. 27. Effect of turbine inlet pressure on system first law thermal efficiency, at $T_c=35^0C$ and $x_2=1$.

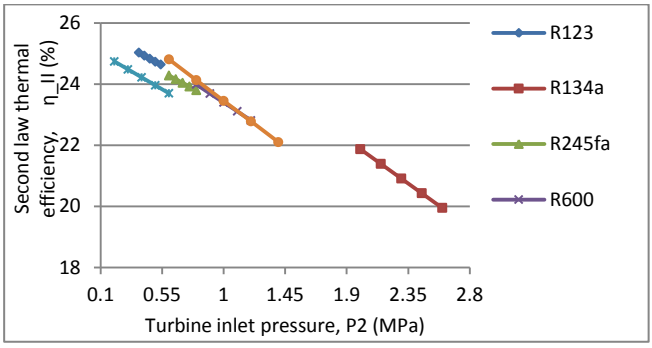

Fig. 28. Effect of turbine inlet pressure on system's second law thermal efficiency, at $T_c=35^0C$ and $x_2=1$.

The effect of turbine inlet pressure on the total system exergy destruction rate was also studied the results are presented in Fig. 29. It can be observed that the exergy destruction rate increases with increasing turbine inlet pressure for all the fluids. The total exergy destruction rate is the sum of the exergy destruction rate in each component. R134a has the highest irreversibility (7.253 kW) and R123 has the lowest (5.775 kW). In general, the turbine contributes more than 41% of the total ORC system irreversibility for all the fluids.

The variation of turbine inlet pressure has minor effect on turbine exit flow rate and system mass flow rate, as presented in Figs. 30 and 31 respectively. Density of the fluid determines the volume flow rate.

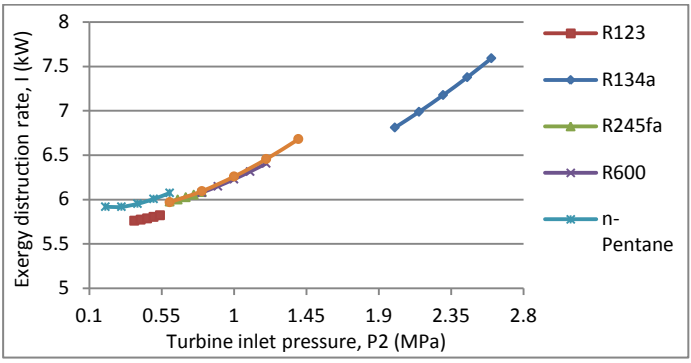

Fig. 29. Effect of turbine inlet pressure on exergy destruction rate, $T_c=35^0C$ & $x_2=1$.

Again, R134a has the least turbine out flow volume flow rate and highest mass flow rate over the pressure range considered. This is because R134a has high density, and high density leads to low turbine exit volume flow rate [13]. This is very important in reducing component size and system cost. n-Pentane has the highest turbine exit volume flow rate and the least mass flow rate.

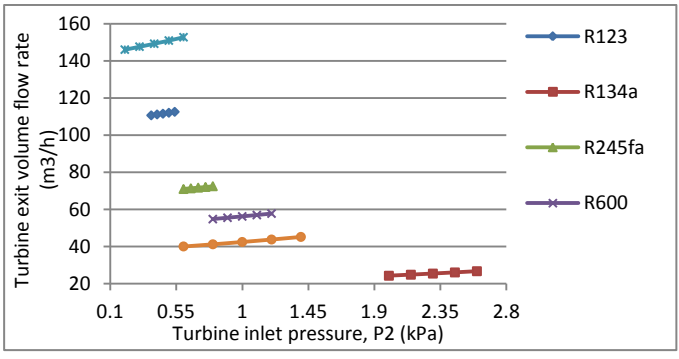

Fig. 30. Effect of turbine inlet pressure on turbine exit volume flow rate, $T_c=35^0C$ and $x_2=1$.

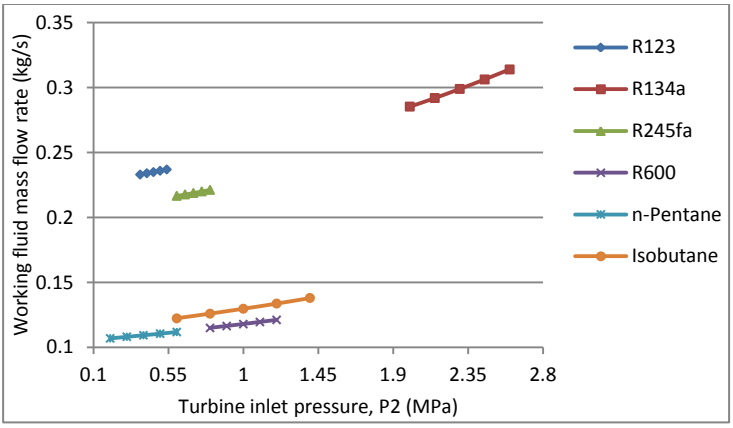

Fig. 31. Effect of turbine inlet pressure on ORC's mass flow rate, $T_c=35^0C$ and $x_2=1$.

Fig. 32 shows the effect of turbine inlet pressure on the ORC heat input rate. Unlike turbine inlet temperature, the heat input rate increases with increasing turbine inlet pressure for all fluids. This is because, as the pressure increases, the latent heat of vaporization decreases.

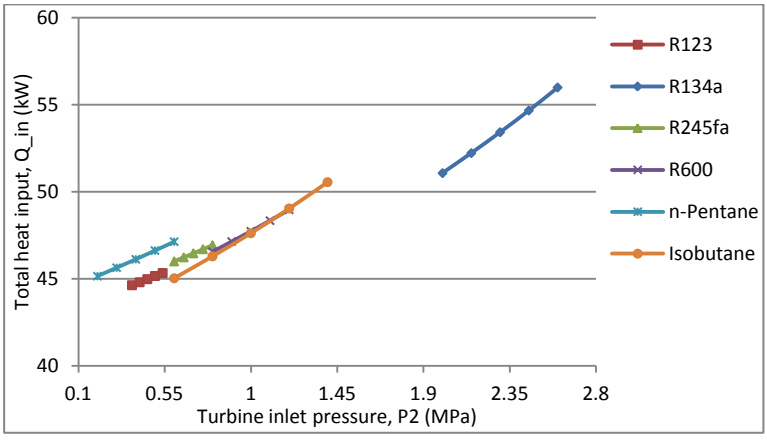

Fig. 32. Effect of turbine inlet pressure on total heat input, $T_c=35^0C$ and $x_2=1$.

5. Conclusion and future work

5.1. Conclusion

This report presented two technologies for conversion of low grade heat: the Stirling engine and the organic Rankine cycle. Based on the thermodynamics study conducted on both systems the following conclusions can be made.

For Stirling engine:

- ✓ Increasing the hot side temperature increases the thermal efficiency, the total heat input and the net work output significantly.
- ✓ Stirling engine with higher regenerator effectiveness value reduces the total heat input, hence increase the thermal efficiency.
- ✓ Increased dead volumes and low regenerator effectiveness has a negative impact on thermal efficiency.
- ✓ Higher phase angle between the hot and cold piston reduces the total heat input and the net work output.

For ORC:

- ✓ For all the fluids tested, increasing the evaporator temperature has economic as well as thermodynamic advantages. High evaporator temperature decreases the exergy destruction rate, the required heat input and the working gas mass flow rate. As a result of these, the first and second law thermal efficiencies increase. It also lowers the volume flow rate at the exit of the turbine, which in turn requires small size turbine, and, therefore lowers the overall cost.
- ✓ Increasing the evaporator pressure has a negative effect on the ORC performance. It increases the heat input and the exergy destruction rate as a result the thermal efficiency decreases for all the fluids.
- ✓ Increasing evaporator pressure also increases the volume flow rate at the expander exit and the working gas mass flow rate.

- ✓ Among the different fluid tested R123 has the highest efficiency and lowest heat input and exergy destruction rate followed by n-Pentane, R245fa, R600, isobutane and R134a. But fluid R134a has the lowest turbine exit volume flow rate followed by isobutane and R600. Therefore, the selection of ORC fluid is a tradeoff between cost and performance.

In general, in terms of their thermodynamics performance both technologies are feasible for conversion of low grade heat in to power (electricity). The choice between the two technologies lies on the temperature of available low grade heat and the required power output.

5.2. Future work

In the present study many simplifying assumptions were made to ease the analysis of both Stirling engine as well as the ORC system. The assumptions made in the analysis of Stirling engine are more general and realistic. Therefore the following points should be considered for future work:

- ✓ The Stirling engine can be modeled with second order analysis, i.e. assuming adiabatic process and including heat conduction in the regenerator.
- ✓ Numerical study can be performed for the heat storage tank of the solar thermal system to improve the hear storage capacity.
- ✓ For ORC, more organic working fluids can be studied for the given heat source temperature of the solar thermal system.

References

[1]. Wongwises S, Kongtragool B. Thermodynamic analysis of a Stirling engine including dead volumes of hot space, cold space and regenerator. Renewable Energy, Vol. 31, pp. 345-359, 2006.

[2]. Li T, Tang D, Li Z, Du J, Zhou T, Jia Y. Development and test of a Stirling engine driven by waste gases for the micro-CHP system. Applied Thermal Engineering Vol. 33-34, pp. 119-123, 2012.

[3]. Cheng, C-H., Yang, H-S. Analytical model for predicting the effect of operating speed on shaft power output of Stirling engines. Energy, Vol. 36, pp. 5899-5908, 2011.

[4]. Wei D, Lu X, Lu Z, Gu J. Dynamic modeling and simulation of an Organic Rankine Cycle (ORC) system for waste heat recovery. Applied Thermal Engineering Vol. 28, pp. 1216-1224, 2008.

[5]. Wang J, Yan Z, Wang M, Ma S, Dai Y. Thermodynamic analysis and optimization of an (organic Rankine cycle) ORC using low grade heat source. Energy Vol. 49, pp. 356-365, 2013.

[6]. Pikra K, Salim A, Prawara B, Purwanto AJ, Admono T, Eddy Z. Development of small scale concentrated solar power plant using organic Rankine cycle for isolated region in Indonesia. Energy Procedia Vol. 32, pp. 122-128, 2013.

[7] Calise F, Capuozzo C, Vanoli L. Design and parametric optimization of an organic Rankine cycle powered by solar energy. American Journal of Engineering and Applied Sciences, Vol. 6, pp. 178-204, 2013.

[8] Liu B-T, Chien K-H, Wang C-C. Effect of working fluids on organic Rankine cycle for waste heat recovery. Energy Vol. 29, pp. 1207-1217, 2004.

[9] Hettiarachchi HDM, Golubovic M, Worek WM, Ikegami Y. Optimum design criteria for an Organic Rankine cycle using low-temperature geothermal heat sources. Energy Vol. 32, pp. 1698-1706, 2007.

[10] Jing L, Gang P, Jie J. Optimization of low temperature solar thermal electric generation with organic Rankine cycle in different areas. Applied Energy Vol. 87, pp. 3355-3365, 2010.

[11] Qiu G. Selection of working fluids for micro-CHP systems with ORC. Renewable Energy Vol. 48, pp. 565-570, 2012.

[12] Aljundi I H. Effect of dry hydrocarbons and critical point temperature on the efficiencies of organic Rankine cycle. Renewable Energy Vol. 36, pp. 1196-1202, 2011.

[13] Bao J, Zhao L. A review of working fluid and expander selections for organic Rankine cycle. Renewable and Sustainable Energy Reviews Vol. 24, pp. 325-342, 2013.

[14] Nag PK, Gupta AVSSKS. Exergy analysis of the Kalina cycle. Applied Thermal Engineering Vol. 18, pp. 427-439, 1998.

[15] Rogdakis E, Antonopoulos K. A high efficiency NH3/H2O absorption power cycle. Heat Recovery Systems and CHP Vol. 11, pp. 263-275, 1991.

[16] Ibrahim MB, Kovach RM. A Kalina cycle application for power generation. Energy Vol. 18, pp. 961-969, 1993.

[17] Lolos P, and Rogdakis E. A Kalina power cycle driven by renewable energy sources. Energy Vol. 34, pp. 457-464, 2009

[18] Dejfors C, Thorin E, Svedberg G. Ammonia-water power cycles for direct-fired cogeneration applications. Energy Conversion and Management Vol. 39, pp. 1675-1681, 1998.

[19] Goswami cycle: http://www.eng.usf.edu/~hchen4/Goswami%20Cycle.htm [Taken on 24/3/2014].

[20] DiPippo R. Second law assessment of binary plants generating power from low-temperature geothermal fluids. Geothermics Vol.33, pp. 565-586, 2004.

[21] Thombare DG, Verma SK. Technological development in the Stirling cycle engine. Renewable and Sustainable Energy Reviews, Vol. 12, pp. 1-38, 2008.

[22] Kongtragool B, Wongwises S. A review of solar-powered Stirling engines and low temperature differential Stirling engines. Renewable and Sustainable Energy Reviews, Vol. 7, pp. 131-154, 2003.

[23] Sripakagom A, Srikam C. Design and performance of a moderate temperature difference Stirling engine. Renewable Energy, Vol. 36, pp. 1728-1733, 2011.

[24] Minassians AD, Sanders SR. Stirling engines for distributed low-cost solar-thermal-electric power generation. Journal of Solar Energy Engineering Vol. 133, pp. 011015 1-10, 2011.

[25] Howard D, Harley RG. Modeling of dish-Stirling solar thermal power generation. IEEE 2010.

[26] Hsu ST, Lin FY, Chiou JS. Heat-transfer aspects of Stirling power generation using incinerator waste energy. Renewable Energy, Vol. 28, pp. 59-69, 2003.

[27] Podesser E. Electric production in rural village with a biomass Stirling engine. Renewable Energy, Vol. 16, pp. 1049-1052, 1999.

[28] Dyson RW, Wilson S, Tew RC. Review of computational Stirling analysis method. Second International Energy Conversion Engineering Conference, August 2004, Rhode Island.

[29] Asnaghi A, Ladjevardi SM, Izadkhast PS, Kashani AH. Thermodydnamic performance analysis of solar Stirling engines. International Scholarly Research Network Vol. 2012, ID 321923.

[30] Ackermann RA. Cryogenic Regenerative heat exchangers. Plenum Press, 1997, New York.

[31] Andersen SK, Carlsen H, Thomsen PG. Numerical study on optimal Stirling engine regenerator matrix designs taking into account the effects of matrix temperature oscillations. Energy Conversion and Management, Vol. 47, pp. 894-908, 2006.

[32] Kays WM, London AL. Compact heat exchangers. McGraw-Hill, 1958, New York.

[33] Klein SA. Engineering Equation Solver, F-Chart Software, 2010, Middleton, WI.

[34]. Shah RK, Sekulic DP. Fundamentals of heat exchanger design. John Wiley & Sons. Inc. 2003, New Jersey.

[35] Finite time thermodynamic evaluation of endoreversible Stirling heat engine at maximum power conditions. Renewable and Sustainable Energy Reviews, Vol. 16, pp. 2234-2241, 2012.

[36] Wang JL, Zhao L, Wang XD. A comparative study of pure and zeotropic mixtures in low-temperature solar Rankine cycle. Applied Energy Vol. 87, pp. 3366-3373, 2010.

[37] Wolpert JL, Riffat SB. Solar-powered Rankine system for domestic applications. Applied Thermal Engineering Vol. 16, pp. 281-289.

[38] Low grade heat conversion: http://www.hindawi.com/journals/mpe/2012/124280/ [Taken on 2/5/2014].

[39] Shengjun Z, Huaixin W, Tao G. Performance comparison and parametric optimization of subcritical organic Rankine cycle (ORC) and transcritical power cycle system for low temperature geothermal power generation. Applied Energy Vol. 88, pp. 2740-2754, 2011.

[40] Chen H, Goswami DY, Stefanakos EK. A review of thermodynamic cycles and working fluids for the conversion of low grade heat. Renewable and Sustainable Energy Reviews Vol. 14, pp. 3059-3067, 2010.

[41] Bandyopadhyay S, Desai NB. Process integration of organic Rankine cycle. Energy Vol. 34, pp. 1674-1686, 2009.

[42] Hung TC, Shai TY, Wang SK. A review of Organic Rankine Cycles (ORC) for the recovery of low-grade waste heat. Energy Vol. 22, No. 7, pp. 661-667, 1997.

[43] Tchanche BF, Papadakis G, Lambrinos G, Frangoudakis A. Fluid selection for a low-temperature solar organic Rankine cycle. Applied Thermal Engineering Vol. 29, pp.2468-2476, 2009.

[44] Wang EH, Zhang HG, Fan BY, Ouyang MG, Zhao Y, Mu QH. Study of working fluid selection of organic Rankine cycle (ORC) for engine waste heat recovery. Energy Vol. 36, pp. 3406-3418, 2011.

[45] Hung T-C. Waste heat recovery of organic Rankine cycle using dry fluids. Energy Conversion and Management Vol. 42, pp. 539-553, 2001.

[46]. Li W, Feng X, Yu LJ, Xu J. Effects of evaporating temperature and internal heat exchanger on organic Rankine cycle. Applied Thermal Engineering Vol. 31, pp. 4014-4023, 2011.

[47] Maizaa V, Maizza A. Unconventional working fluids in organic Rankine-cycles for waste energy recovery systems. Applied Thermal Engineering Vol. 21, pp. 381-390, 2001.

[48] Angelino G, Invernizzi C, Macchi E. Organic working fluid optimization for space power cycles. In: Angelino G, De Luca L, Sirignano WA, editors. Modern research topics in aerospace propulsion. New York: Springer-Verlag; 1991.

[49] Polysun software: http://www.velasolaris.com/english/home.html [Taken on 4/18/2014].

[50] Quoilin S, Orosz M, Hemond H, Lemort V. Performance and design optimization of a low-cost solar organic Rankine cycle for remote power generation. Solar Energy Vol. 85, pp. 955-966, 2011.